# Large carbon cycle sensitivities to climate across a permafrost thaw gradient in subarctic Sweden

Kuang-Yu Chang*,
Climate and Ecosystem Sciences Division, Lawrence Berkeley National Laboratory, Berkeley, California, USA
William J. Riley,
Climate and Ecosystem Sciences Division, Lawrence Berkeley National Laboratory, Berkeley, California, USA
Patrick M. Crill,
Department of Geological Sciences, Stockholm University, Stockholm, Sweden
Robert F. Grant,
Department of Renewable Resources, University of Alberta, Edmonton, Alberta, Canada
Virginia I. Rich,
Department of Microbiology, The Ohio State University, Columbus, Ohio, USA
and,
Scott R. Saleska,
Department of Ecology and Evolutionary Biology, University of Arizona, Tucson, Arizona, USA

*Corresponding author: Kuang-Yu Chang, ckychang@lbl.gov
Climate and Ecosystem Sciences Division, Lawrence Berkeley National Laboratory
Berkeley, California, USA

25 Phone: (510) 495-8141

## Abstract

Permafrost peatlands store large amounts of carbon potentially vulnerable to decomposition. However, the fate of that carbon in a changing climate remains uncertain in models due to complex interactions among hydrological, biogeochemical, microbial, and plant processes. In this study, we estimated effects of climate forcing biases present in global climate reanalysis products on carbon cycle predictions at a thawing permafrost peatland in subarctic Sweden. The analysis was conducted with a comprehensive biogeochemical model (*ecosys*) across a permafrost thaw gradient encompassing intact permafrost palsa with an ice core and a shallow active layer, partly thawed bog with a deeper active layer and a variable water table, and fen with a water table close to the surface, each with distinct vegetation and microbiota. Using *in situ* observations to correct local cold and wet biases found in the Global Soil Wetness Project Phase 3 (GSWP3) climate reanalysis forcing, we demonstrate good model performance by comparing predicted and observed carbon dioxide ($CO_2$) and methane ($CH_4$) exchanges, thaw depth, and water table depth. The simulations driven by the bias-corrected climate suggest that the three peatland types currently accumulate carbon from the atmosphere, although the bog and fen sites can have annual positive radiative forcing impacts due to their higher $CH_4$ emissions. Our simulations indicate that projected precipitation increases could accelerate $CH_4$ emissions from the palsa area, even without further degradation of palsa permafrost. The GSWP3 cold and wet biases for this site significantly alter simulation results and lead to erroneous active layer depth (ALD) and carbon budget estimates. Biases in simulated $CO_2$ and $CH_4$ exchanges from biased climate forcing are as large as those among the thaw stages themselves at a landscape-scale across the

examined permafrost thaw gradient. Future studies should thus not only focus on changes in carbon budget associated with morphological changes in thawing permafrost, but also recognize the effects of climate forcing uncertainty on carbon cycling.

## 1. Introduction

Confidence in future climate projections depends on the accuracy of terrestrial carbon budget estimates, which are presently very uncertain (Friedlingstein et al., 2014; Arneth et al., 2017). In addition to the complexity in physical process representations, a major source of this uncertainty comes from challenges in quantifying climate responses induced by biogeochemical feedbacks. Increases in atmospheric carbon dioxide ($CO_2$) concentrations can directly stimulate carbon sequestration from plant photosynthesis (Cox et al., 2000; Friedlingstein et al., 2006) and indirectly stimulate carbon emissions (e.g., from soil warming and resulting increased respiration), although the predicted magnitudes of these exchanges strongly depend on model process representations (Zaehle et al., 2010; Grant, 2013, 2014; Ghimire et al., 2016; Chang et al, 2018).

The undecomposed carbon stored in permafrost is of critical importance for biogeochemical feedbacks to climate because it is about twice as much as currently is in the atmosphere (Hugelius et al., 2014) and is vulnerable to release to the atmosphere as permafrost thaws (Schuur et al., 2015). O'Donnell et al. (2012) suggested that permafrost thaw would result in a net loss of soil organic carbon from the entire peat column because accumulation rates at the surface were insufficient to balance deep soil organic carbon losses upon thaw. Jones et al. (2017) indicated that the loss of sporadic and discontinuous permafrost by 2100 could result in a release of up to 24 Pg of soil carbon from permafrost peatlands to the atmosphere. Lundin et al. (2016) reported that it is plausible (71% probability) for the subarctic landscapes to serve as a net carbon source to the atmosphere while its peatland components being atmospheric carbon sinks, which highlights the importance of spatial heterogeneity on high latitude carbon budget estimation.

In addition to the overall carbon balance of the changing Arctic, the type of carbon gaseous emission is important to climate feedbacks. High latitudes are predicted to get wetter (IPCC, 2014), and saturated anaerobic conditions facilitate methane ($CH_4$) production, which is a much more efficient greenhouse gas than $CO_2$ in terms of global warming potential. Even habitats that can be net carbon sinks can produce positive radiative forcing impacts on climate due to $CH_4$ release, as Bäckstrand et al. (2010) showed for a subarctic peatland. Under projected warming and wetting trends in the Arctic (Collins et al., 2013; Bintanja and Andry, 2017), carbon cycle feedbacks over the permafrost region could become stronger as increased precipitation enhances surface permafrost thaw and strengthens $CH_4$ emissions by expansion of anaerobic volume (Christensen et al., 2004; Wickland et al., 2006).

The Stordalen Mire in northern Sweden (68.20°N, 19.03°E) is in the discontinuous permafrost zone, encompassing a mosaic of thaw stages with associated distinct hydrology and vegetation (Christensen et al. 2004; Malmer et al., 2005), microbiota (Mondav and Woodcroft et al., 2014; Mondav et al., 2017; Woodcroft and Singleton et al., 2018), and organic matter chemistry (Hodgkins et al., 2014). These landscapes have been shifting over the last half-century to a more thawed state, likely due to recent warming (Christensen et al. 2004). Drier hummock sites dominated by shrubs have degraded to wetter sites dominated by graminoids (Malmer et al., 2005; Johansson et al., 2006). The thaw-induced habitat shifts are associated with increases in landscape-scale $CH_4$ emissions (Christensen et al. 2004; Johansson et al., 2006; Cooper et al., 2017) reflective of the higher $CH_4$ emissions of the wetter thawed habitats (McCalley et al., 2014). The higher $CO_2$ uptake in later thaw-stage habitats has not compensated for the

98 increase in positive radiative forcing from elevated $CH_4$ emissions (Bäckstrand et al.,
99 2010; Deng et al., 2014).
100 The impacts of climate sensitivity on the terrestrial carbon cycle have been
101 investigated at the global scale, and the results highlight the need to consider uncertainty
102 in climate datasets when evaluating permafrost region carbon cycle simulations
103 (Ahlström et al., 2017; Guo et al., 2017; Wu et al., 2017). Ahlström et al. (2017) showed
104 that climate forcing biases are responsible for a considerable fraction (~40%) of the
105 uncertainty range in ecosystem carbon predictions from 18 Earth System Models (ESMs)
106 reported by Anav et al. (2013). Guo et al. (2017) concluded that the differences in climate
107 forcing contribute to significant differences in simulated soil temperature, permafrost
108 area, and Active Layer Depth (ALD). Wu et al. (2017) demonstrated that differences
109 among climate forcing datasets contributes more to predictive uncertainty than
110 differences in apparent model sensitivity to climate forcing. However, notably, none of
111 these studies accessed the effects on $CH_4$ emissions, and their spatial resolution could not
112 represent site-level spatial heterogeneity observed in arctic tundra (Grant et al. 2017a;
113 2017b).
114 Here, we use the ecosystem model *ecosys*, which employs a comprehensive set of
115 coupled biogeochemical and hydrological processes, to estimate the effects of climate
116 forcing uncertainty and sensitivity on $CO_2$ and $CH_4$ exchanges and thaw depth
117 simulations. For the Stordalen Mire site, we estimated bias in the Global Soil Wetness
118 Project Phase 3 (GSWP3) climate reanalysis dataset using site-level long-term
119 meteorological measurements and evaluated impacts on simulated soil and plant
120 processes across the permafrost thaw gradient. This approach enables us to assess model

121 sensitivity to individual climate forcing biases, instead of the aggregated uncertainty
122 range embedded in climate datasets (e.g., variations of climate conditions represented in
123 different climate datasets) presented in previous studies. We address the following
124 questions for our study site at the Stordalen Mire: (1) What are the biases embedded in
125 the GSWP3 climate reanalysis dataset? (2) How do those biases affect model predictions
126 of thaw depth, $CO_2$ exchanges, and $CH_4$ exchanges? (3) How does climate sensitivity
127 vary across the stages of permafrost thaw? In addition to improving understanding of
128 permafrost responses to climate, we identify ecosystem carbon prediction uncertainty
129 induced by climate forcing uncertainty in general as the biases found in GSWP3 were
130 consistent with other climate reanalysis datasets during the last decade (section 3).
131
132 **2. Methods and Data**
133 **2.1 Study site description**
134 Our study sites are located at the Stordalen Mire (68.20 °N, 19.03 °E: 351 m
135 above sea level), which is about 10 km southeast of the Abisko Scientific Research
136 Station (ANS) in northern Sweden. The Stordalen Mire is in the discontinuous permafrost
137 zone along the 0 °C isotherm where permafrost at low elevations primarily presents in
138 peatlands, bordered by lakes to the northwest and southeast (Kokfelt et al., 2010). A large
139 portion of the mire consists of a slightly elevated drained area underlain by permafrost
140 characterized by a hummocky topography, and the remaining portion is largely lacking
141 permafrost with fen-like conditions (Johansson et al., 2006). The recent warming (more
142 than 1 °C) has deepened the mean ALD measured at the Stordalen Mire by around 20 cm
143 since the early 1980's, accompanied by palsa collapses and thermokarst erosion

(Christensen et al., 2004; Malmer et al., 2005; Johansson et al., 2006). Specifically, the mean ALD has increased from 0.48 m to 0.63 m in the drier part of the mire and from 0.63 m to 0.86 m in the wetter part, from September 1973–1976 (Rydén and Kostov, 1980) to September 2003–2005 (Johansson et al., 2006).

Significant changes in climate over this region have been recorded during the last few decades. The annual mean air temperature measured at the ANS has risen by 2.5 °C from 1913 to 2006, where it exceeded the 0 °C threshold (0.6 °C in 2006) for the first time over the past century (Callaghan et al., 2010). The measured annual total precipitation has also increased from 306 mm $y^{-1}$ (years 1913 to 2009) to 336 mm $y^{-1}$ (years 1980 to 2009) (Olefeldt and Roulet, 2012), along with increased variability in extreme precipitation (Callaghan et al., 2010). The measured annual maximum snow depth has increased from 59 cm (years 1957 to 1971) to 70 cm (years 1986 to 2000), however, the snow cover period with snow depth greater than 20 cm has decreased from 5.8 months (years 1957 to 1971) to 4.9 months (years 1986 to 2000) (Malmer et al., 2005).

Inception of peat deposition at the Stordalen Mire has been dated at around 6,000 calendar years before present (cal. BP) (Sonesson 1972) in the southern part of the mire and at around 4,700 cal. BP in the northern part (Kokfelt et al., 2010). Kokfelt et al. (2010) suggested that permafrost aggregation initiated during the Little Ice Age (around 120–400 cal. BP) in the Stordalen Mire. At present, the Stordalen Mire can be broadly classified into three peatland types: intact permafrost palsa, partly thawed bog, and fen (Hodgkins et al., 2014), hereafter referred to as palsa, bog, and fen (Figure 1). The spatial distribution of these peatland types in 2000 are described in Olefeldt and Roulet (2012).

Based on Swedish military photography, all three of the investigated peatland types have existed since at least the 1930's. The palsa sites are ombrotrophic and raised 0.5 to 2.0 m above their surroundings, with a relatively thin peat layer (0.4 to 0.7 m, Rydén et al., 1980), thinner active layer depth (less than 0.7 m in late summer), and no measurable water table depth (Bäckstrand et al., 2008a; 2008b; Olefeldt and Roulet, 2012). The bog sites are ombrotrophic and are wetter than the palsa sites, with a thicker peat layer (0.5 to ~1 m, Rydén et al., 1980), deeper ALD (greater than 0.9 m, the deepest measurement depth), and water table depth fluctuating from 35 cm below the peat surface to the ground surface (Bäckstrand et al., 2008a; 2008b; Olefeldt and Roulet, 2012). The fen sites are minerotrophic, receiving a large amount of water from a lake to the east of the mire, with water table depths near or above the ground surface (Bäckstrand et al., 2008a; 2008b; Olefeldt and Roulet, 2012).

Differences in hydrology and permafrost conditions create high spatial heterogeneity with different soil moisture, pH, and nutrient conditions that support different plant communities (Bäckstrand et al., 2008a; 2008b). The palsa is dominated by dwarf shrubs with some sedges, feather mosses, and lichens (Malmer et al., 2005; Bäckstrand et al., 2008a; 2008b; Olefeldt and Roulet, 2012). The bog is dominated by *Sphagnum* spp. mosses with a moderate abundance of sedges (Malmer et al., 2005; Bäckstrand et al., 2008a; 2008b; Olefeldt and Roulet, 2012). The fen sites we studied are dominated by sedges (Bäckstrand et al., 2008a; 2008b).

**2.2 Field measurements**

189 Continuous daily meteorological measurements have been recorded at the ANS
190 since 1913, including air temperature, precipitation, wind speed, wind direction, relative
191 humidity, and snow depth. Measurements of solar radiation, longwave radiation, and soil
192 temperature are also available at the ANS since 1982. The soil thaw depth (measured to
193 90 cm) and water table depth measurements were taken in the three peatland types 3 to 5
194 times per week from early May to mid-October during 2003 to 2007 (Bäckstrand et al.,
195 2008b).
196 $CO_2$ and $CH_4$ exchanges at the three peatland types were measured with
197 automated chambers during the thawed seasons from 2002 to 2007 (Bäckstrand et al.,
198 2008b). Chamber lids were removed when snow accumulates in winter (around
199 November), and the sampling periods for each year ranged from 60 days (28 March (day
200 87) to 27 May (day 147)) in 2002 (shortest) to 193 days (28 May (day 148) to 7
201 December (day 341)) (longest) (Bäckstrand et al., 2008b; Bäckstrand et al., 2010). Three
202 chambers were installed in the palsa, another three in the bog, and two more in the fen
203 (we term each chamber a 'subsite' in the following). Each chamber covered an area of
204 0.14 $m^2$ with a height of 25–45 cm depending on the vegetation and the depth of insertion
205 and was closed for 5 minutes every 3 hours to measure $CO_2$ and total hydrocarbon (THC)
206 exchanges. $CH_4$ exchanges were manually observed approximately 3 times per week, and
207 these measurements were used to quantify the proportion of $CH_4$ in the measured THC
208 (Bäckstrand et al., 2008a). The $CH_4$ exchanges were near zero in the palsa sites
209 (Bäckstrand et al., 2008a; Bäckstrand et al., 2008b; Bäckstrand et al., 2010), so they were
210 not used in model evaluation. We used the $CO_2$ and $CH_4$ exchanges observed at 3-hourly
211 steps when the $R^2$ values recorded in the measurements were greater than 0.8 (Tokida et

al., 2007), and then calculated the associated daily mean exchanges when there were 8 measurements per day (Table 1). The quality-controlled daily measurements only covered 12.4–33.7% of the daily data points because of the lack of continuous quality-controlled 3-hourly measurements. The data screening was applied to exclude unreliable measurements and avoid biases from inappropriate gap filling, which is necessary for model evaluations. More detailed descriptions of the $CO_2$ and $CH_4$ exchanges measurements can be found in Bäckstrand et al. (2008a).

### 2.3 GSWP3

GSWP3 is an ongoing modeling activity that provides global gridded meteorological forcing (0.5° x 0.5° resolution) and investigates changes in energy, water, and carbon cycles throughout the 20$^{th}$ and 21$^{st}$ centuries. The GSWP3 dataset is based on the 20$^{th}$ Century Reanalysis (Compo et al., 2011), using a spectral nudging dynamical downscaling technique described in Yoshimura and Kanamitsu (2008). A more detailed description of the GSWP can be found in Dirmeyer (2011) and van den Hurk et al. (2016).

In this study, we extracted the meteorological conditions at the Stordalen Mire from 1901 to 2010 from the GSWP3 climate reanalysis dataset. The 3-hourly products of air temperature, precipitation, solar radiation, wind speed, and specific humidity were interpolated to hourly intervals with cubic spline interpolation to serve as the meteorological inputs used in our model.

The GSWP3 dataset was chosen over other existing climate reanalysis datasets for its spatial and temporal resolutions. For example, the Climatic Research Unit (CRU;

Harris et al., 2014) dataset provided monthly meteorological forcing at 0.5° x 0.5° resolution; the National Centers for Environmental Prediction (NCEP; Kalnay et al., 1996; Kanamitsu et al., 2002) dataset provided 6-hourly meteorological forcing at T62 Gaussian grid (~1.915° x 1.895° resolution); the CRUNCEP (Viovy, 2018) dataset provided 6-hourly meteorological forcing at 0.5° x 0.5° resolution; and the European Centre for Medium-Range Weather Forecasts (ECMWF; Berrisford et al., 2011) dataset provided 3-hourly meteorological forcing with 125 km (~1.125°) horizontal resolution.

**2.4 Model description**

*Ecosys* is a comprehensive biogeochemistry model that simulates ecosystem responses to diverse environmental conditions with explicit representations of microbial dynamics and soil carbon, nitrogen, and phosphorus biogeochemistry. The above-ground processes are represented in multi-layer plant interacting canopies that are allowed to change with changing environmental conditions, and the below-ground processes are represented in multiple soil layers with multi-phase subsurface reactive transport. *Ecosys* operates at variable time steps (down to seconds) determined by convergence criteria, and it can be applied at patch scale (spatially homogenous one-dimensional) and landscape-scale (spatially variable two- or three-dimensional). Detailed descriptions, including inputs, outputs, governing equations, parameters, and references of the *ecosys* model can be found in Grant (2013). A qualitative summery of the *ecosys* model structure is provided in the supplemental material to this article.

The *ecosys* model has been extensively tested against eddy covariance fluxes and related ecophysiological measurements with a wide range of sites and weather conditions

in boreal, temperate, and tropical forests (Grant et al., 2007a; Grant et al., 2007c; Grant et al., 2009a; Grant et al., 2009b; Grant et al., 2009c; Grant et al., 2010), wetlands (Dimitrov et al., 2011; Grant et al., 2012b; Dimitrov et al., 2014; Mezbahuddin et al., 2014), grasslands (Grant and Flanagan, 2007; Grant et al., 2012a), tundra (Grant et al., 2003; Grant et al., 2011b; Grant 2015; Grant et al., 2015), croplands (Grant et al., 2007b; Grant et al., 2011a), and other permafrost-associated habitats (Grant and Roulet, 2002; Grant, 2017a; Grant et al., 2017b). All *ecosys* model structures are unchanged from those described in these earlier studies.

**2.5 Experimental design**

To evaluate the effects of climate on model predictions, we conducted four sets of simulations at each of the three peatland types at the Stordalen Mire from 1901 to 2010. The climate data from 1901 to 2001 were used for model initialization (i.e., spinup) and those from 2002 to 2010 were used for analysis. The 110 year simulations were performed to ensure the simulation was equilibrated with local climate (Grant et al. 2017a).

The meteorological conditions for all the simulations were based on the hourly data extracted from the GSWP3 climate reanalysis dataset (section 2.3). The monthly mean bias of the GSWP3 for this location was calculated by comparing it to the air temperature and precipitation measured at the ANS, for years 1913 to 2010 (section 3.1). The full series of air temperature and precipitation extracted from GSWP3 were then bias-corrected using the monthly mean bias calculated from 1913 to 2010; we label this model scenario CTRL. Our bias correction was conceptually similar to the one used in Ahlström et al. (2017), where the bias-corrected climate forcing fields were the ESM

281 outputs adjusted by the corresponding bias calculated from observations in a reference
282 period.
283 The simulation results from CTRL should represent the reliability of applying
284 *ecosys* at the Stordalen Mire because CTRL is driven by the best local climate
285 description. We first evaluated predicted thaw depth, water table depth, and $CO_2$ and $CH_4$
286 exchanges using the CTRL simulation (section 3.2 to 3.4). In the second set of
287 simulations, BIASED-COLD, the biased GSWP3 air temperature data was used, and we
288 corrected only the GSWP3 precipitation. Deviations between CTRL and BIASED-COLD
289 reflect biased air temperature's effects on responses across the thaw gradient. In the third
290 set of simulations, BIASED-WET, we bias-corrected the air temperature extracted from
291 GSWP3, which allows us to quantify the effects of biased precipitation. Finally, we used
292 the meteorological conditions directly extracted from GSWP3 to drive our fourth set of
293 simulations, BIASED-COLD&BIASED-WET, which reveals the uncertainty range of
294 subarctic peatland simulation associated with the local biases in GSWP3 climate forcing.
295 While the three peatland types share the same climate conditions, they differ in
296 soil hydrologic conditions and vegetation characteristics (section 2.1; Figure 1). The bulk
297 density and porosity profiles were set to the values reported in Rydén et al. (1980), who
298 suggested a decreasing trend of bulk density and an increasing trend of porosity from
299 palsa (0.12 $Mgm^{-3}$ at surface; 92–93% within the upper 10 cm) to bog and fen (0.06
300 $Mgm^{-3}$ at surface; 96–97% within the upper 10 cm). The peatland soil carbon-to-nitrogen
301 (CN) ratios and pH values were assigned according to Hodgkins et al. (2014), who
302 documented an increasing trend of pH from palsa (4.0), to bog (4.2), to fen (5.7), and a
303 decreasing trend of soil organic matter CN ratio from bog (46±18), to palsa (39±24), to

fen (19±0.4). Common values of field capacity (0.4) and wilting point (0.15) were used for the three peatland types (Deng et al., 2014). The soil property and vegetation parameters used in our simulation for the three peatland types are summarized in Supplemental Material Table1 and Supplemental Material Table2, respectively.

## 3 Results and Discussion

### 3.1 GSWP3 climate comparison to observations

As described in section 2.3, we extracted meteorological conditions at the Stordalen Mire from the GSWP3 climate reanalysis dataset. The closest GSWP3 grid cell was centered at 68.0 °N and19.0 °E, which covers the Stordalen Mire and the ANS. The annual mean air temperature and precipitation calculated at this GSWP3 grid cell were -3.65 °C and 683.88 mm $y^{-1}$, respectively, for years 1913 to 2010. A cold bias (-3.09 °C) was identified in the GSWP3 annual mean air temperature during the 1913 to 2010 period, although a very high correlation coefficient (r = 0.99) was found when compared with the ANS measurements (Figure 2a). Both time series exhibit an overall warming trend from the early 20$^{th}$ century to the present (0.01°C $y^{-1}$), with an even larger warming trend from 1980 to 2010 (0.05 °C $y^{-1}$ [ANS] and 0.04 °C $y^{-1}$ [GSWP3]).

Similarly, the GSWP3 annual total precipitation data correlates well with ANS measurements (r = 0.80) but has a wet bias of 380 mm $y^{-1}$ between 1913 and 2010 (Figure 2b). An increasing trend in annual total precipitation was recorded in both time series from the early 20$^{th}$ century to present (0.47 mm $y^{-2}$ [ANS] and 1.07 mm $y^{-2}$ [GSWP3]), although a decreasing trend was found from 1980 to 2010 (-0.56 mm $y^{-2}$ [ANS] and -2.39 mm $y^{-2}$ [GSWP3]).

The seasonal cycle of the GSWP3 monthly mean air temperature also matches that measured at the ANS, with a very high correlation coefficient (r = 0.99; Figure 3a). The underestimation bias and inter-annual variability of GSWP3 air temperature are greater in winter (maximum underestimate in December, at -4.52 °C with inter-annual variability of 3.53 °C) and smaller in summer (minimum underestimate in July, at -1.52 °C with inter-annual variability of 1.65 °C), respectively.

The magnitude and inter-annual variability of the GSWP3 monthly mean precipitation are comparable between winter and summer, while the ANS measurements exhibit stronger seasonality with lower magnitudes during winter. Despite the differences found in seasonal patterns, a high correlation coefficient (r = 0.64) was found between the monthly mean precipitation extracted from GSWP3 and the ANS measurements. The overestimation of monthly mean precipitation was greatest in December (43.25 mm month$^{-1}$) and smallest in August (18.75 mm month$^{-1}$).

These comparisons suggest that GSPW3 air temperature and precipitation data reasonably capture measured seasonal and long-term trends over past decades, but are biased cold and wet compared to observations, especially during winter. Similar cold and wet biases exist in CRUNCEP and ECMWF climate reanalysis datasets during our 2003 to 2007 study period (Supplemental Material Figure 1). The annual mean air temperature and precipitation at the Stordalen Mire for years 2003 to 2007 were -2.49 °C and 795.09 mm y$^{-1}$; -2.46 °C and 708.60 mm y$^{-1}$; and -2.28 °C and 765.67 mm y$^{-1}$ in the GSWP3, CRUNCEP, and ECMWF climate reanalysis datasets, respectively.

**3.2 Model testing**

### 3.2.1 Thaw depth

We first evaluated *ecosys* against observations using bias-corrected climate forcing (i.e., the CTRL simulation). Predicted thaw depth agrees well with measurements collected from 2003 to 2007 for all examined peatland types (Figure 4), with a correlation coefficient of 0.95, 0.87, and 0.41 at the palsa, bog, and fen, respectively. Both simulations and observations show that the rate of thaw depth deepening in the summer varies with peatland type (i.e., relatively slow, moderate, and rapid in the palsa, bog, and fen, respectively).

Predicted and observed maximum thaw depths (i.e., ALD) in the intact permafrost palsa were between 45 and 60 cm in September. In the partly thawed bog, the simulated thaw depth is slightly shallower than that observed before August. The simulated bog thaw depth exceeds 90 cm by the end of August, which matches the time when measured thaw depth reaches its maximum. In contrast, the thaw depth exceeds 90 cm nearly one month earlier in the fen. The patterns of thawing permafrost presented here are consistent with Deng et al. (2014), who simulated the same site using the DNDC model.

### 3.2.2 $CO_2$ exchanges

The daily Net Ecosystem Exchange (NEE) simulated in the CTRL simulation reasonably captures observed seasonal dynamics from 2003 to 2007 for all the examined peatland types (Figure 5). The simulations and observations generally showed net $CO_2$ uptake (with some episodic $CO_2$ emissions) during summer and release during winter. The observations and simulations also showed large $CO_2$ emissions in the palsa site during fall of 2004. Simulated fall $CO_2$ bursts in the three sites in other years could not be

373 confirmed because of a lack of observations during these periods. Similar to the patterns
374 reported in Raz-Yaseef et al. (2016), some episodic $CO_2$ emission pulses were simulated
375 as surface ice thaws in spring, but there were no measurements to confirm those events.
376 The correlation coefficients of the simulated and observed daily NEE ranged from 0.58 to
377 0.60, and most of the discrepancies between the simulations and observations were within
378 the ranges of NEE variability measured at different subsites (automated chambers) within
379 the same peatland type. The simulated $CO_2$ uptake rates in the bog were greater than the
380 observations in summer, which could be due to overestimated plant biomass or
381 overestimated $CO_2$ uptake rate per plant biomass. However, we currently do not have
382 data to examine the cause of this overestimation because the $CO_2$ flux derived from
383 automated chambers only represents the aggregated results of all controlling factors.
384 As described in section 2.2, simulated $CO_2$ exchanges were evaluated for 3-hourly
385 and daily time steps when quality-controlled measurements were available ($R^2$ values and
386 relative root mean squared errors (RRMSEs) shown in Table 2). Simulated NEE is in
387 reasonable agreement with the 3-hourly NEE measurements with RRMSEs ranging
388 from 8.4 to 19.1%. Model comparisons with observations were generally poorer at daily
389 time steps, although the calculated RRMSEs were comparable to those reported in Deng
390 et al. (2014). We suspect these differences resulted from uncertainty in determining an
391 accurate observed daily NEE that is representative of the entire peatland type. This may
392 be due to: (1) limited daily data points (less than 14% across the study period, Table 1)
393 due to lack of continuous quality-controlled 3-hourly measurements; and (2) the large
394 variability of daily NEE ranges measured at different subsites within the same peatland
395 type (Figure 5). Our results thus indicate that NEE is affected by thaw stage (Bäckstrand

et al., 2010; Deng et al., 2014) and fine scale spatial heterogeneity of the system. More detailed measurements with higher spatial and temporal resolutions within the same peatland type would be necessary to characterize the effects of this type of heterogeneity.

### 3.2.3 Water table depth and $CH_4$ exchanges

Simulated water table depth generally captures observed seasonal patterns measured in the bog and fen sites from 2003 to 2007 (Figure 6a, c). During summer, the predicted bog water table depth fluctuates around the ground surface (-7 to -1 cm), and the predicted water table depth is at or above the ground surface in the fen. Water table depths simulated by *ecosys* are generally higher than measured in the bog, where measured water table depths are often below the ground surface with greater seasonal variability. Simulated fen water table depths have better overall fit to observations, being higher (~5 cm) than measurements in 2003 and 2004, close to measurements in 2005 and 2006, and slightly deeper (~2 cm) than measurements in 2007. These differences in modeled and observed water table depth could be driven by the limitations of our one-dimensional column simulation that could not resolve topographic effects and thus hinder the variations of water table depth, which is a particular issue in simulating the dynamic water table of the bog. For example, no excessive water could be transported to the neighboring grids to deepen local water table depth under our current model configuration. A multi-dimensional simulation that includes realistic topographic effects could help improve the representation of water table dynamics, and estimates of the measurement uncertainty would help facilitate the assessment of simulation bias.

418 Simulated and measured daily $CH_4$ exchanges correlate reasonably well in the
419 bog (r = 0.49) and well in the fen (r = 0.65) across the study period (Figure 6b, d). Both
420 the simulations and observations have stronger $CH_4$ emissions during summer with peak
421 emissions in late summer. Some episodic $CH_4$ emission pulses (Mastepanov et al., 2008)
422 were simulated during shoulder seasons, and the simulated amount of post-growing
423 season $CH_4$ emissions agrees well with those measured in 2007.
424 Most of the discrepancies between simulated and observed $CH_4$ emissions were
425 within the variability of measurements across subsites within the same peatland type. The
426 3-hourly and daily RRMSEs ranged from 11.1 to 22.3% (Table 2) and the daily RRMSEs
427 were comparable to results presented in Deng et al. (2014). Our results show that model
428 evaluation of $CH_4$ emissions with finer temporal resolution observations is not necessarily
429 superior to evaluation with coarser temporal resolution, as compared to the NEE
430 counterpart, which could be related to comparatively lesser $CH_4$ emission variability
431 measured across subsites within the same peatland type (Figure 6b, d).
432
433 **3.3 Variability across the permafrost thaw gradient**
434 Thaw rate and ALD increase along the thaw gradient (i.e., palsa to bog to fen),
435 and landscape variations are generally greater than simulated inter-annual variability
436 (Figure 7a). Maximum carbon uptake also increases along the thaw gradient, and
437 variations across the landscape are comparable with simulated intra-seasonal and inter-
438 annual variabilities (Figure 7b). The simulated mean seasonal cumulative NEE were
439 calculated based on the seasonality identified in Bäckstrand et al. (2010) to help facilitate
440 the inter-comparison of carbon budgets estimated at the Stordalen Mire, and to better

capture the actual seasonality recorded at the study site. The results show that the magnitude of mean growing season $CO_2$ uptake is highest in the fen and lowest in the palsa (Table 3). The same rank applies to the magnitude of mean $CO_2$ emissions over the non-growing season, although differences across the thaw gradient are smaller.

$CH_4$ emission rates increase significantly along the thaw gradient, and the palsa site emissions are negligible (Figure 7c). Mean cumulative $CH_4$ emissions simulated in the fen are much higher than those in the bog, and most $CH_4$ emissions occur during the growing season (Table 3). The higher $CH_4$ emissions in the fen can be attributed to its faster seasonal thaw rate (Figure 7a) and a water table depth close to the surface (Figure 6c). Seasonal cumulative NEE and $CH_4$ emissions from observations could not be accessed due to the lack of continuous quality controlled carbon flux measurements during our study period (Table 1).

### 3.4 Climate sensitivity of permafrost thaw

#### 3.4.1 Thaw responses to climate

Our results indicate that the ALD currently simulated in the bog and fen is around 108 cm and 130 cm, respectively. However, the maximum depth of our thaw depth measurements is 90 cm, which makes it difficult to evaluate our model performance on ALD simulation. Our results highlight the need to acquire measurements at deeper depth to resolve whether there is no permafrost currently remaining in the bog and fen, or there is a talik with permafrost developed deeper than the simulated ALDs. Such information could be important in predicting microbial activity and thermokarst in permafrost

463 peatlands (Schuur et al., 2015), but it may not significantly alter the effects of climate
464 forcing uncertainty discussed in our study.

465 For each of the four sets of simulations with different climate forcing (section
466 2.5), simulated mean ALD from 2003 to 2007 is always greatest in the fen and lowest in
467 the palsa (Figure 8). This consistent trend along the thaw gradient indicates that ALDs
468 are largely regulated by their distinct ecological and hydrological conditions, because all
469 three sites had the same climate forcing in each set of simulations (i.e., CTRL, BIASED-
470 COLD, BIASED-WET, and BIASED-COLD&BIASED-WET). Therefore, the palsa,
471 bog, and fen have different resilience against the changes in climate forcing, and this type
472 of ecosystem resilience plays an important role in determining ALD under changes in
473 climate conditions.

474 Effects of climate on simulated ALD are similar across peatland types (Figure 8).
475 With increased precipitation (BIASED-WET vs. CTRL), simulated ALD generally
476 becomes deeper with greater inter-annual variability because the increased snowpack
477 depth keeps the soil warmer with lower soil ice content during winter. This effect is less
478 prominent in the comparison between experiments BIASED-COLD and BIASED-
479 COLD&BIASED-WET, because the cold biases in these two experiments (section 3.1)
480 constrain thaw depth development. For example, summertime soil heating in some of the
481 simulation years was not strong enough to thaw the soil ice between 20-40 cm completely
482 in the BIASED-COLD&BIASED-WET run, resulting in shallower ALDs simulated in
483 the palsa and fen even with the snowpack warming effect. The simulated ALD also
484 becomes deeper with higher air temperature (CTRL vs. BIASED-COLD; BIASED-WET
485 vs. BIASED-COLD&BIASED-WET) at all the examined peatland types. This response

is more evident in the comparison between experiments BIASED-WET and BIASED-COLD&BIASED-WET, probably driven by their wet biases (section 3.1) that facilitate thaw depth deepening (via increased thermal conductivity and advective heat transport; Grant et al. 2017a). Similar dependencies between ALD and climate were shown in Åkerman and Johansson (2008) and Johansson et al. (2013), based on multi-year measurements and snow manipulation experiments.

Therefore, the combined cold and wet biases in the GSWP3 climate reanalysis dataset could counteract their individual effects on simulated ALD development at the Stordalen Mire. Our results indicate a 28.6%, 0.7%, and 11.7% underestimation of ALD simulated in the palsa, bog, and fen, respectively, when applying the GSWP3 climate reanalysis data over this region without proper bias correction (BIASED-COLD&BIASED-WET vs. CTRL). Our sensitivity analysis suggests that projected warming and wetting trends (Collins et al., 2013) could significantly increase ALD in the Arctic, since increases in precipitation and air temperature can both contribute to ALD deepening.

### 3.4.2 Carbon budget responses to climate

Simulations with the four climate forcing datasets (section 2.5) indicate annual mean (from 2003 to 2007) $CO_2$ sinks and $CH_4$ sources, except the weak $CO_2$ emissions simulated in the fen in experiment BIASED-COLD&BIASED-WET due to reduced sedge productivity driven by increased temperature and oxygen stresses (Figure 9a,b). Our results also indicate that differences in annual $CO_2$ and $CH_4$ exchanges across the four climate forcing datasets for a single peatland type are as large as those across

509 peatland types for a single climate forcing dataset (Figure 9a,b). These large $CO_2$ and
510 $CH_4$ exchanges climate sensitivities demonstrate that the peatland's dynamical responses
511 to climate have stronger effects on the carbon cycle than on ALDs (Figure 8).
512 With bias-corrected precipitation, increased air temperature (CTRL vs. BIASED-
513 COLD) leads to stronger $CO_2$ uptake and greater $CH_4$ emissions at all the examined
514 peatland types (Figure 9a,b), mainly because enhanced sedge growth facilitates carbon
515 cycling under a warmer environment (results not shown). This air temperature sensitivity
516 affects $CO_2$ and $CH_4$ exchanges within the same peatland type without significantly
517 changing ALD (Figure 8). For both experiments, $CO_2$ uptake and $CH_4$ emissions are
518 greatest in the fen and lowest in the palsa, consistent with the measurements reported in
519 Bäckstrand et al. (2010) for the same period. Based on the Coupled Model
520 Intercomparison Project, phase 5 (CMIP5) ESM simulations, arctic annual mean surface
521 air temperature is projected to increase by 8.5±2.1 °C over the 21$^{st}$ century (Bintanja and
522 Andry, 2017). This projected air temperature increase is more than double the air
523 temperature difference between site-observed and GSWP3 temperatures, which could
524 significantly enhance $CH_4$ emissions regardless of palsa degradation into bog and fen.
525 On the other hand, wet biases (BIASED-WET and BIASED-COLD&BIASED-
526 WET) increase $CH_4$ emissions in the palsa; wetter and colder conditions result in as much
527 $CH_4$ release as the current fen, while wetter conditions alone drive palsa emissions
528 comparable to the current bog (Figure 9b). The large precipitation sensitivity found in
529 palsa $CH_4$ emissions could have strong effects on palsa carbon cycling because arctic
530 precipitation is projected to increase by 50 – 60% towards the end of the 21$^{st}$ century
531 (based on CMIP5 estimates; Bintanja and Andry, 2017). The comparison between

532 experiments BIASED-WET and BIASED-COLD&BIASED-WET shows that in the
533 palsa, increased air temperature strengthens $CO_2$ uptake and weakens $CH_4$ emissions.
534 This shift is primarily driven in the model by increased shrub and moss productivity
535 under the warmer environment, which facilitate $CO_2$ uptake while drying out the soil and
536 reducing $CH_4$ emissions (results not shown). In the bog and fen sites, increased air
537 temperature under wet bias strengthens both the simulated $CO_2$ uptake and $CH_4$
538 emissions (BIASED-WET vs. BIASED-COLD&BIASED-WET), due to enhanced sedge
539 growth under the warmer environment that facilitates carbon cycling in the experiment
540 BIASED-WET. The low $CH_4$ emissions in bog and fen simulated in experiment
541 BIASED-COLD&BIASED-WET are driven by increased temperature and oxygen
542 stresses that greatly reduce heterotrophic respiration ($CH_4$ production) and sedge cover
543 (aerenchyma transport).

544 We assessed the integrated effects of the changes in $CO_2$ and $CH_4$ exchanges
545 identified in the full suite of simulations in terms of the Net Carbon Balance (NCB) and
546 net emissions of greenhouse gases expressed as $CO_2$ equivalents (Net Greenhouse Gas
547 Balance; NGGB). NCB was defined as the sum of the annual total $CO_2$ and $CH_4$
548 exchanges. NGGB was defined in a similar fashion as the NCB, but considers the greater
549 radiative forcing potential of $CH_4$ than $CO_2$ (28 times over a 100-year horizon, Myhre et
550 al., 2013) when calculating the annual total. The calculated NCB values are mostly
551 negative because the stronger $CO_2$ uptake dominates the weaker $CH_4$ emissions (Figure
552 9c). The results suggest that all the examined peatland types serve as net carbon sinks
553 under current climate (CTRL), consistent with the estimates reported in Deng et al.
554 (2014) and Lundin et al. (2016). We find a 24, 36, and 38 g C $m^{-2}$ $y^{-1}$ underestimation of

555 NCB simulated in the palsa, bog, and fen sites, respectively, due to the cold and wet
556 biases in the GSWP3 climate reanalysis dataset (BIASED-COLD&BIASED-WET vs.
557 CTRL). NGGB is affected more strongly by $CH_4$ emissions (Figure 9d) due to its larger
558 radiative forcing potential. NGGB values are positive over the bog and fen, suggesting
559 that these sites have positive radiative forcing impacts despite being net carbon sinks.
560 NGGB simulated in the palsa is generally negative (i.e., a net sink from the atmosphere)
561 due to lower $CH_4$ emissions, except for the simulation conducted without any climate bias
562 correction (correcting only air temperature increased $CH_4$ emissions but not enough to
563 compensate for the significantly higher $CO_2$ sink). Our results indicate that the simulated
564 NGGB would be biased by 298, -66, and -252 g $CO_2$-eq $m^{-2}$ $y^{-1}$ in the palsa, bog, and fen,
565 respectively, without proper bias correction for the GSWP3 climate reanalysis dataset
566 (BIASED-COLD&BIASED-WET vs. CTRL). Using the GSWP3 products directly thus
567 effectively eliminates the positive radiative forcing from the expanding bog and fen,
568 while creating a potentially dramatically inaccurate positive radiative forcing from the
569 shrinking palsa.
570
571 **3.4.3 Climate sensitivity versus landscape heterogeneity**
572 Climate sensitivity and landscape heterogeneity are defined here as variability
573 across the four climate forcing datasets for a single peatland type, and variability across
574 three peatland types with bias-corrected climate (CTRL), respectively. We estimated
575 carbon cycle variability associated with climate sensitivity and landscape heterogeneity to
576 quantify the corresponding uncertainty in our annual carbon cycle assessments from 2003
577 to 2007. Our results indicate that differences in simulated annual mean $CO_2$ exchanges

578 and NCB from climate sensitivity are greater than those from landscape heterogeneity
579 (Figure 9a,c); i.e., annual $CO_2$ uptake strength is more sensitive to climate forcing
580 uncertainty than to peatland type representation. In terms of the simulated annual mean
581 $CH_4$ emissions and NGGB, our results indicate that variability from climate sensitivity is
582 comparable to those from landscape heterogeneity (Figure 9b,d). Therefore, bias-
583 corrected climate and realistic peatland characterization are both necessary to reduce the
584 uncertainty in representing carbon cycling dynamics and their radiative forcing effects.
585 In addition to their effects on carbon cycle predictions, changes in climate
586 conditions also affect permafrost degradation and thus induce changes in areal cover of
587 peatland types. Malmer et al. (2005) showed that there were -0.95, 0.24, and 0.62 ha areal
588 cover changes (-10.3%, 4.0%, and 46.3% percentage changes) from 1970 to 2000 in
589 palsa, bog, and fen, respectively, at the Stordalen Mire. By applying the annual mean
590 $CO_2$ and $CH_4$ exchanges simulated with bias-corrected climate from 2003 to 2007, the
591 areal cover changes from 1970 to 2000 alone would lead to -44 kg C $y^{-1}$, 76 kg C $y^{-1}$, and
592 2076 kg $CO_2$-eq $y^{-1}$ changes in annual mean $CO_2$ exchanges, $CH_4$ exchanges, and NGGB,
593 respectively, at the Stordalen Mire. The changes in landscape-scale carbon cycle
594 dynamics indicate that the radiative warming impact of increased $CH_4$ emissions is large
595 enough to offset the radiative cooling impact of increased $CO_2$ uptake at the Stordalen
596 Mire, consistent with the estimates reported in Deng et al. (2014). The areal cover
597 changes across peatland types could persist or accelerate under the projected warming
598 and wetting trends in the Arctic (Collins et al., 2013; Bintanja and Andry, 2017), which
599 could stimulate $CH_4$ emissions and produce a stronger radiative warming impact.
600

## 4. Conclusions

We evaluated the climate bias in a widely used atmospheric reanalysis product (GSWP3) at our northern Sweden Stordalen Mire site. We then applied a comprehensive biogeochemistry model, *ecosys*, to estimate the effects of these biases on active layer development and carbon cycling across a thaw gradient at the site. Our results show that *ecosys* reasonably represented measured hydrological, thermal, and biogeochemical cycle processes in the intact permafrost palsa, partly thawed bog, and fen. We found that the cold and wet biases in the GSWP3 climate reanalysis dataset significantly alter model simulations, leading to biases in simulated Active Layer Depths, Net Carbon Balance, and Net Greenhouse Gas Balance by up to 28.6%, 38 g C $m^{-2}$ $y^{-1}$, and 298 g $CO_2$-eq $m^{-2}$ $y^{-1}$, respectively. The Net Carbon Balance simulated with bias-corrected climate suggests that all the examined peatland types are currently net carbon sinks from the atmosphere, although the bog and fen sites can have positive radiative forcing impacts due to their higher $CH_4$ emissions.

Our results indicate that the annual means of ALD, $CO_2$ uptake, and $CH_4$ emissions generally increase along the permafrost thaw gradient at the Stordalen Mire under current climate, consistent with previous studies in this region. Our analysis suggests that palsa, bog, and fen differ strongly in their carbon cycling dynamics and have different responses to climate forcing biases. Differences in simulated $CO_2$ and $CH_4$ exchanges driven by uncertainty from climate forcing are as large as those from landscape heterogeneity across the examined permafrost thaw gradient. Model simulations demonstrate that the palsa site exhibits the strongest sensitivity to biases in air temperature and precipitation. The wet bias in GSWP3 could erroneously increase

predicted $CH_4$ emissions from the palsa site to a magnitude comparable to emissions currently measured in the bog and fen sites. These results also show that increased precipitation projected for high latitude regions could strongly accelerate $CH_4$ emissions from the palsa area, even without degradation of palsa into bog and fen. Future studies should thus recognize the effects of climate forcing uncertainty on carbon cycling, in addition to tracking changes in carbon budgets associated with areal changes in permafrost degradation.

**Acknowledgements**

This study was funded by the Genomic Science Program of the United States Department of Energy Office of Biological and Environmental Research under the ISOGENIE project, grant DE-SC0016440, to Lawrence Berkeley Laboratory under contract DE-AC02-05CH11231, and by support from the Swedish Research Council (VR) to PMC. We thank the Abisko Scientific Research Station of the Swedish Polar Research Secretariat for providing the meteorological data. We are furthermore thankful to the two anonymous reviewers who provided constructive comments that improved the manuscript.

642 **References**

643 Ahlström, A., Schurgers, G. and Smith, B.: The large influence of climate model bias on
644 terrestrial carbon cycle simulations, Environmental Research Letters, 12(1),
645 014004, doi:10.1088/1748-9326/12/1/014004, 2017.
646 Anav, A., Friedlingstein, P., Kidston, M., Bopp, L., Ciais, P., Cox, P., Jones, C., Jung,
647 M., Myneni, R. and Zhu, Z.: Evaluating the Land and Ocean Components of the
648 Global Carbon Cycle in the CMIP5 Earth System Models, J. Climate, 26(18),
649 6801–6843, doi:10.1175/JCLI-D-12-00417.1, 2013.
650 Arneth, A., Sitch, S., Pongratz, J., Stocker, B. D., Ciais, P., Poulter, B., Bayer, A. D.,
651 Bondeau, A., Calle, L., Chini, L. P., Gasser, T., Fader, M., Friedlingstein, P.,
652 Kato, E., Li, W., Lindeskog, M., Nabel, J. E. M. S., Pugh, T. A. M., Robertson,
653 E., Viovy, N., Yue, C. and Zaehle, S.: Historical carbon dioxide emissions caused
654 by land-use changes are possibly larger than assumed, Nature Geoscience, 10(2),
655 79–84, doi:10.1038/ngeo2882, 2017.
656 Bäckstrand, K., Crill, P. M., Mastepanov, M., Christensen, T. R. and Bastviken, D.: Non-
657 methane volatile organic compound flux from a subarctic mire in Northern
658 Sweden, Tellus B, 60(2), 226–237, doi:10.1111/j.1600-0889.2007.00331.x,
659 2008a.
660 Bäckstrand, K., Crill, P. M., Mastepanov, M., Christensen, T. R. and Bastviken, D.: Total
661 hydrocarbon flux dynamics at a subarctic mire in northern Sweden, Journal of
662 Geophysical Research: Biogeosciences, 113(G3), doi:10.1029/2008JG000703,
663 2008b.

664 Backstrand, K., Crill, P. M., ski, M. J.-K., Mastepanov, M., Christensen, T. R. and
665 Bastviken, D.: Annual carbon gas budget for a subarctic peatland, Northern
666 Sweden, 14, 2010.
667 Berrisford, P., Dee, D. P., Poli, P., Brugge, R., Fielding, K., Fuentes, M., Kållberg, P. W.,
668 Kobayashi, S., Uppala, S. and Simmons, A.: The ERA-Interim archive Version
669 2.0, 2011.
670 Bintanja, R. and Andry, O.: Towards a rain-dominated Arctic, Nature Climate Change,
671 7(4), 263–267, doi:10.1038/nclimate3240, 2017.
672 Callaghan, T. V., Bergholm, F., Christensen, T. R., Jonasson, C., Kokfelt, U. and
673 Johansson, M.: A new climate era in the sub-Arctic: Accelerating climate changes
674 and multiple impacts, Geophysical Research Letters, 37(14),
675 doi:10.1029/2009GL042064, 2010.
676 Chang, K.-Y., Paw U, K. T. and Chen, S.-H.: The importance of carbon-nitrogen
677 biogeochemistry on water vapor and carbon fluxes as elucidated by a multiple
678 canopy layer higher order closure land surface model, Agricultural and Forest
679 Meteorology, 259, 60–74, doi:10.1016/j.agrformet.2018.04.009, 2018.
680 Christensen, T. R., Johansson, T., Åkerman, H. J., Mastepanov, M., Malmer, N., Friborg,
681 T., Crill, P. and Svensson, B. H.: Thawing sub-arctic permafrost: Effects on
682 vegetation and methane emissions, Geophysical Research Letters, 31(4),
683 doi:10.1029/2003GL018680, 2004.
684 Collins, M., R. Knutti, J. Arblaster, J.-L. Dufresne, T. Fichefet, P. Friedlingstein, X. Gao,
685 W.J. Gutowski, T. Johns, G. Krinner, M. Shongwe, C. Tebaldi, A.J. Weaver and
686 M. Wehner, 2013: Long-term Climate Change: Projections, Commitments and

687 Irreversibility. Climate Change 2013: The Physical Science Basis. Contribution of
688 Working Group I to the Fifth Assessment Report of the Intergovernmental Panel
689 on Climate Change. T. F. Stocker et al., Eds., Cambridge University Press, 1029-
690 1136.
691 Compo, G. P., Whitaker, J. S., Sardeshmukh, P. D., Matsui, N., Allan, R. J., Yin, X.,
692 Gleason, B. E., Vose, R. S., Rutledge, G., Bessemoulin, P., Brönnimann, S.,
693 Brunet, M., Crouthamel, R. I., Grant, A. N., Groisman, P. Y., Jones, P. D., Kruk,
694 M. C., Kruger, A. C., Marshall, G. J., Maugeri, M., Mok, H. Y., Nordli, Ø., Ross,
695 T. F., Trigo, R. M., Wang, X. L., Woodruff, S. D. and Worley, S. J.: The
696 Twentieth Century Reanalysis Project, Quarterly Journal of the Royal
697 Meteorological Society, 137(654), 1–28, doi:10.1002/qj.776, 2011.
698 Cooper, M. D. A., Estop-Aragonés, C., Fisher, J. P., Thierry, A., Garnett, M. H.,
699 Charman, D. J., Murton, J. B., Phoenix, G. K., Treharne, R., Kokelj, S. V., Wolfe,
700 S. A., Lewkowicz, A. G., Williams, M. and Hartley, I. P.: Limited contribution of
701 permafrost carbon to methane release from thawing peatlands, Nature Climate
702 Change, 7(7), 507–511, doi:10.1038/nclimate3328, 2017.
703 Cox, P. M., Betts, R. A., Jones, C. D., Spall, S. A. and Totterdell, I. J.: Acceleration of
704 global warming due to carbon-cycle feedbacks in a coupled climate model, 408,
705 4, 2000.
706 Deng, J., Li, C., Frolking, S., Zhang, Y., Bäckstrand, K. and Crill, P.: Assessing effects of
707 permafrost thaw on C fluxes based on multiyear modeling across a permafrost
708 thaw gradient at Stordalen, Sweden, Biogeosciences, 11(17), 4753–4770,
709 doi:10.5194/bg-11-4753-2014, 2014.

710 Dimitrov, D. D., Bhatti, J. S. and Grant, R. F.: The transition zones (ecotone) between
711 boreal forests and peatlands: Ecological controls on ecosystem productivity along
712 a transition zone between upland black spruce forest and a poor forested fen in
713 central Saskatchewan, Ecological Modelling, 291, 96–108,
714 doi:10.1016/j.ecolmodel.2014.07.020, 2014.
715 Dimitrov Dimitre D., Grant Robert F., Lafleur Peter M. and Humphreys Elyn R.:
716 Modeling the effects of hydrology on gross primary productivity and net
717 ecosystem productivity at Mer Bleue bog, Journal of Geophysical Research:
718 Biogeosciences, 116(G4), doi:10.1029/2010JG001586, 2011.
719 Dirmeyer, P. A.: A History and Review of the Global Soil Wetness Project (GSWP),
720 Journal of Hydrometeorology, 12(5), 729–749, doi:10.1175/JHM-D-10-05010.1,
721 2011.
722 Friedlingstein, P., Cox, P., Betts, R., Bopp, L., von Bloh, W., Brovkin, V., Cadule, P.,
723 Doney, S., Eby, M., Fung, I., Bala, G., John, J., Jones, C., Joos, F., Kato, T.,
724 Kawamiya, M., Knorr, W., Lindsay, K., Matthews, H. D., Raddatz, T., Rayner, P.,
725 Reick, C., Roeckner, E., Schnitzler, K.-G., Schnur, R., Strassmann, K., Weaver,
726 A. J., Yoshikawa, C. and Zeng, N.: Climate–Carbon Cycle Feedback Analysis:
727 Results from the C $^{4}$ MIP Model Intercomparison, Journal of Climate, 19(14),
728 3337–3353, doi:10.1175/JCLI3800.1, 2006.
729 Friedlingstein, P., Meinshausen, M., Arora, V. K., Jones, C. D., Anav, A., Liddicoat, S.
730 K. and Knutti, R.: Uncertainties in CMIP5 Climate Projections due to Carbon
731 Cycle Feedbacks, Journal of Climate, 27(2), 511–526, doi:10.1175/JCLI-D-12-
732 00579.1, 2014.

733 Ghimire, B., Riley, W. J., Koven, C. D., Mu, M. and Randerson, J. T.: Representing leaf
734 and root physiological traits in CLM improves global carbon and nitrogen cycling
735 predictions, Journal of Advances in Modeling Earth Systems, 8(2), 598–613,
736 doi:10.1002/2015MS000538, 2016.
737 Grant, R. F.: Modelling changes in nitrogen cycling to sustain increases in forest
738 productivity under elevated atmospheric CO2 and contrasting site conditions,
739 Biogeosciences, 10(11), 7703–7721, doi:10.5194/bg-10-7703-2013, 2013.
740 Grant, R. F.: Nitrogen mineralization drives the response of forest productivity to soil
741 warming: Modelling in ecosys vs. measurements from the Harvard soil heating
742 experiment, Ecological Modelling, 288, 38–46,
743 doi:10.1016/j.ecolmodel.2014.05.015, 2014.
744 Grant R. F. and Flanagan L. B.: Modeling stomatal and nonstomatal effects of water
745 deficits on CO2 fixation in a semiarid grassland, Journal of Geophysical
746 Research: Biogeosciences, 112(G3), doi:10.1029/2006JG000302, 2007.
747 Grant, R. F. and Roulet, N. T.: Methane efflux from boreal wetlands: Theory and testing
748 of the ecosystem model Ecosys with chamber and tower flux measurements,
749 Global Biogeochemical Cycles, 16(4), 2-1-2–16, doi:10.1029/2001GB001702,
750 2002.
751 Grant, R. F., Oechel, W. C. and Ping, C.-L.: Modelling carbon balances of coastal arctic
752 tundra under changing climate, Global Change Biology, 9(1), 16–36,
753 doi:10.1046/j.1365-2486.2003.00549.x, 2003.
754 Grant, R. F., Black, T. A., Humphreys, E. R. and Morgenstern, K.: Changes in net
755 ecosystem productivity with forest age following clearcutting of a coastal

Douglas-fir forest: testing a mathematical model with eddy covariance measurements along a forest chronosequence, Tree Physiol., 27(1), 115–131, 2007a.

Grant, R. F., Arkebauer, T. J., Dobermann, A., Hubbard, K. G., Schimelfenig, T. T., Suyker, A. E., Verma, S. B. and Walters, D. T.: Net Biome Productivity of Irrigated and Rainfed Maize–Soybean Rotations: Modeling vs. Measurements, Agronomy Journal, 99(6), 1404, doi:10.2134/agronj2006.0308, 2007b.

Grant, R. F., Barr, A. G., Black, T. A., Gaumont□Guay, D., Iwashita, H., Kidson, J., McCAUGHEY, H., Morgenstern, K., Murayama, S., Nesic, Z., Saigusa, N., Shashkov, A. and Zha, T.: Net ecosystem productivity of boreal jack pine stands regenerating from clearcutting under current and future climates, Global Change Biology, 13(7), 1423–1440, doi:10.1111/j.1365-2486.2007.01363.x, 2007c.

Grant, R. F., Margolis, H. A., Barr, A. G., Black, T. A., Dunn, A. L., Bernier, P. Y. and Bergeron, O.: Changes in net ecosystem productivity of boreal black spruce stands in response to changes in temperature at diurnal and seasonal time scales, Tree Physiology, 29(1), 1–17, doi:10.1093/treephys/tpn004, 2009a.

Grant, R. F., Barr, A. G., Black, T. A., Margolis, H. A., Dunn, A. L., Metsaranta, J., Wang, S., McCaughey, J. H. and Bourque, C. A.: Interannual variation in net ecosystem productivity of Canadian forests as affected by regional weather patterns – A Fluxnet-Canada synthesis, Agricultural and Forest Meteorology, 149(11), 2022–2039, doi:10.1016/j.agrformet.2009.07.010, 2009b.

Grant, R. F., Hutyra, L. R., Oliveira, R. C., Munger, J. W., Saleska, S. R. and Wofsy, S. C.: Modeling the carbon balance of Amazonian rain forests: resolving ecological

779 controls on net ecosystem productivity, Ecological Monographs, 79(3), 445–463,
780 doi:10.1890/08-0074.1, 2009c.
781 Grant, R. F., Barr, A. G., Black, T. A., Margolis, H. A., Mccaughey, J. H. and Trofymow,
782 J. A.: Net ecosystem productivity of temperate and boreal forests after
783 clearcutting—a Fluxnet-Canada measurement and modelling synthesis, Tellus B:
784 Chemical and Physical Meteorology, 62(5), 475–496, doi:10.1111/j.1600-
785 0889.2010.00500.x, 2010.
786 Grant, R. F., Kimball, B. A., Conley, M. M., White, J. W., Wall, G. W. and Ottman, M.
787 J.: Controlled Warming Effects on Wheat Growth and Yield: Field Measurements
788 and Modeling, Agronomy Journal, 103(6), 1742–1754,
789 doi:10.2134/agronj2011.0158, 2011a.
790 Grant, R. F., Humphreys, E. R., Lafleur, P. M. and Dimitrov, D. D.: Ecological controls
791 on net ecosystem productivity of a mesic arctic tundra under current and future
792 climates, Journal of Geophysical Research: Biogeosciences, 116(G1),
793 doi:10.1029/2010JG001555, 2011b.
794 Grant, R. F., Baldocchi, D. D. and Ma, S.: Ecological controls on net ecosystem
795 productivity of a seasonally dry annual grassland under current and future
796 climates: Modelling with ecosys, Agricultural and Forest Meteorology, 152, 189–
797 200, doi:10.1016/j.agrformet.2011.09.012, 2012a.
798 Grant, R. F., Desai, A. R. and Sulman, B. N.: Modelling contrasting responses of wetland
799 productivity to changes in water table depth, Biogeosciences, 9(11), 4215–4231,
800 doi:10.5194/bg-9-4215-2012, 2012b.

Grant R. F., Humphreys E. R. and Lafleur P. M.: Ecosystem CO2 and CH4 exchange in a mixed tundra and a fen within a hydrologically diverse Arctic landscape: 1. Modeling versus measurements, Journal of Geophysical Research: Biogeosciences, 120(7), 1366–1387, doi:10.1002/2014JG002888, 2015.

Grant, R. F., Mekonnen, Z. A., Riley, W. J., Wainwright, H. M., Graham, D. and Torn, M. S.: Mathematical Modelling of Arctic Polygonal Tundra with Ecosys: 1. Microtopography Determines How Active Layer Depths Respond to Changes in Temperature and Precipitation, Journal of Geophysical Research: Biogeosciences, 122(12), 3161–3173, doi:10.1002/2017JG004035, 2017a.

Grant, R. F., Mekonnen, Z. A., Riley, W. J., Arora, B. and Torn, M. S.: Mathematical Modelling of Arctic Polygonal Tundra with *Ecosys:* 2. Microtopography Determines How $CO_2$ and $CH_4$ Exchange Responds to Changes in Temperature and Precipitation: GHG Exchange in Arctic Polygonal Tundra, Journal of Geophysical Research: Biogeosciences, 122(12), 3174–3187, doi:10.1002/2017JG004037, 2017b.

Guo, D., Wang, H. and Wang, A.: Sensitivity of Historical Simulation of the Permafrost to Different Atmospheric Forcing Data Sets from 1979 to 2009, Journal of Geophysical Research: Atmospheres, 122(22), 12,269-12,284, doi:10.1002/2017JD027477, 2017.

Harris, I., Jones, P. D., Osborn, T. J. and Lister, D. H.: Updated high-resolution grids of monthly climatic observations – the CRU TS3.10 Dataset, International Journal of Climatology, 34(3), 623–642, doi:10.1002/joc.3711, n.d.

Hodgkins, S. B., Tfaily, M. M., McCalley, C. K., Logan, T. A., Crill, P. M., Saleska, S. R., Rich, V. I. and Chanton, J. P.: Changes in peat chemistry associated with permafrost thaw increase greenhouse gas production, Proceedings of the National Academy of Sciences, 111(16), 5819–5824, doi:10.1073/pnas.1314641111, 2014.

van den Hurk, B., Kim, H., Krinner, G., Seneviratne, S. I., Derksen, C., Oki, T., Douville, H., Colin, J., Ducharne, A., Cheruy, F., Viovy, N., Puma, M. J., Wada, Y., Li, W., Jia, B., Alessandri, A., Lawrence, D. M., Weedon, G. P., Ellis, R., Hagemann, S., Mao, J., Flanner, M. G., Zampieri, M., Materia, S., Law, R. M. and Sheffield, J.: LS3MIP (v1.0) contribution to CMIP6: the Land Surface, Snow and Soil moisture Model Intercomparison Project – aims, setup and expected outcome, Geoscientific Model Development, 9(8), 2809–2832, doi:10.5194/gmd-9-2809-2016, 2016.

Hugelius, G., Strauss, J., Zubrzycki, S., Harden, J. W., Schuur, E. A. G., Ping, C.-L., Schirrmeister, L., Grosse, G., Michaelson, G. J., Koven, C. D., O'Donnell, J. A., Elberling, B., Mishra, U., Camill, P., Yu, Z., Palmtag, J. and Kuhry, P.: Estimated stocks of circumpolar permafrost carbon with quantified uncertainty ranges and identified data gaps, Biogeosciences, 11(23), 6573–6593, doi:10.5194/bg-11-6573-2014, 2014.

IPCC, 2014: Climate Change 2014: Synthesis Report. Contribution of Working Groups I, II and III to the Fifth Assessment Report of the Intergovernmental Panel on Climate Change [Core Writing Team, R.K. Pachauri and L.A. Meyer (eds.)]. IPCC, Geneva, Switzerland, 151 pp.

845 Johansson, M., Callaghan, T. V., Bosiö, J., Åkerman, H. J., Jackowicz-Korczynski, M.
846 and Christensen, T. R.: Rapid responses of permafrost and vegetation to
847 experimentally increased snow cover in sub-arctic Sweden, Environmental
848 Research Letters, 8(3), 035025, doi:10.1088/1748-9326/8/3/035025, 2013.
849 Johansson, T., Malmer, N., Crill, P. M., Friborg, T., åKerman, J. H., Mastepanov, M. and
850 Christensen, T. R.: Decadal vegetation changes in a northern peatland, greenhouse
851 gas fluxes and net radiative forcing, Global Change Biology, 12(12), 2352–2369,
852 doi:10.1111/j.1365-2486.2006.01267.x, 2006.
853 Jones, M. C., Harden, J., O'Donnell, J., Manies, K., Jorgenson, T., Treat, C. and Ewing,
854 S.: Rapid carbon loss and slow recovery following permafrost thaw in boreal
855 peatlands, Glob. Chang. Biol., 23(3), 1109–1127, doi:10.1111/gcb.13403, 2017.
856 Kalnay, E., Kanamitsu, M., Kistler, R., Collins, W., Deaven, D., Gandin, L., Iredell, M.,
857 Saha, S., White, G., Woollen, J., Zhu, Y., Chelliah, M., Ebisuzaki, W., Higgins,
858 W., Janowiak, J., Mo, K. C., Ropelewski, C., Wang, J., Leetmaa, A., Reynolds,
859 R., Jenne, R. and Joseph, D.: The NCEP/NCAR 40-Year Reanalysis Project, Bull.
860 Amer. Meteor. Soc., 77(3), 437–472, doi:10.1175/1520-
861 0477(1996)077<0437:TNYRP>2.0.CO;2, 1996.
862 Kanamitsu, M., Ebisuzaki, W., Woollen, J., Yang, S.-K., Hnilo, J. J., Fiorino, M. and
863 Potter, G. L.: NCEP–DOE AMIP-II Reanalysis (R-2), Bull. Amer. Meteor. Soc.,
864 83(11), 1631–1644, doi:10.1175/BAMS-83-11-1631, 2002.
865 Kokfelt, U., Reuss, N., Struyf, E., Sonesson, M., Rundgren, M., Skog, G., Rosen, P., and
866 Hammarlund, D.: Wetland development, permafrost history and nutrient cycling

inferred from late Holocene peat and lake sediment records in subarctic Sweden, J. Paleolimn., 44, 327–342, doi:10.1007/s10933-010-9406- 8, 2010.

Lundin, E. J., Klaminder, J., Giesler, R., Persson, A., Olefeldt, D., Heliasz, M., Christensen, T. R. and Karlsson, J.: Is the subarctic landscape still a carbon sink? Evidence from a detailed catchment balance, Geophysical Research Letters, 43(5), 1988–1995, doi:10.1002/2015GL066970, 2016.

Malmer, N., Johansson, T., Olsrud, M. and Christensen, T. R.: Vegetation, climatic changes and net carbon sequestration in a North-Scandinavian subarctic mire over 30 years, Global Change Biology, 11(11), 1895–1909, doi:10.1111/j.1365-2486.2005.01042.x, 2005.

Mastepanov, M., Sigsgaard, C., Dlugokencky, E. J., Houweling, S., Ström, L., Tamstorf, M. P. and Christensen, T. R.: Large tundra methane burst during onset of freezing, Nature, 456(7222), 628–630, doi:10.1038/nature07464, 2008.

McCalley, C. K., Woodcroft, B. J., Hodgkins, S. B., Wehr, R. A., Kim, E.-H., Mondav, R., Crill, P. M., Chanton, J. P., Rich, V. I., Tyson, G. W. and Saleska, S. R.: Methane dynamics regulated by microbial community response to permafrost thaw, Nature, 514(7523), 478–481, doi:10.1038/nature13798, 2014.

Mezbahuddin, M., Grant, R. F. and Hirano, T.: Modelling effects of seasonal variation in water table depth on net ecosystem $CO_2$ exchange of a tropical peatland, Biogeosciences, 11(3), 577–599, doi:10.5194/bg-11-577-2014, 2014.

Mondav, R., McCalley, C. K., Hodgkins, S. B., Frolking, S., Saleska, S. R., Rich, V. I., Chanton, J. P. and Crill, P. M.: Microbial network, phylogenetic diversity and community membership in the active layer across a permafrost thaw gradient,

Environmental Microbiology, 19(8), 3201–3218, doi:10.1111/1462-2920.13809, 2017.

Mondav, R., Woodcroft, B. J., Kim, E.-H., McCalley, C. K., Hodgkins, S. B., Crill, P. M., Chanton, J., Hurst, G. B., VerBerkmoes, N. C., Saleska, S. R., Hugenholtz, P., Rich, V. I. and Tyson, G. W.: Discovery of a novel methanogen prevalent in thawing permafrost, Nature Communications, 5, 3212, doi:10.1038/ncomms4212, 2014.

Myhre, G., D. Shindell, F.-M. Bréon, W. Collins, J. Fuglestvedt, J. Huang, D. Koch, J.-F. Lamarque, D. Lee, B. Mendoza, T. Nakajima, A. Robock, G. Stephens, T. Takemura and H. Zhang, 2013: Anthropogenic and Natural Radiative Forcing. In: Climate Change 2013: The Physical Science Basis. Contribution of Working Group I to the Fifth Assessment Report of the Intergovernmental Panel on Climate Change [Stocker, T.F., D. Qin, G.-K. Plattner, M. Tignor, S.K. Allen, J. Boschung, A. Nauels, Y. Xia, V. Bex and P.M. Midgley (eds.)]. Cambridge University Press, Cambridge, United Kingdom and New York, NY, USA, pp. 659–740, doi:10.1017/ CBO9781107415324.018.

O'Donnell, J. A., Jorgenson, M. T., Harden, J. W., McGuire, A. D., Kanevskiy, M. Z. and Wickland, K. P.: The Effects of Permafrost Thaw on Soil Hydrologic, Thermal, and Carbon Dynamics in an Alaskan Peatland, Ecosystems, 15(2), 213–229, doi:10.1007/s10021-011-9504-0, 2012.

Olefeldt, D. and Roulet, N. T.: Effects of permafrost and hydrology on the composition and transport of dissolved organic carbon in a subarctic peatland complex, Journal

912 of Geophysical Research: Biogeosciences, 117(G1), doi:10.1029/2011JG001819,
913 2012.
914 Piao, S., Liu, Z., Wang, T., Peng, S., Ciais, P., Huang, M., Ahlstrom, A., Burkhart, J. F.,
915 Chevallier, F., Janssens, I. A., Jeong, S.-J., Lin, X., Mao, J., Miller, J.,
916 Mohammat, A., Myneni, R. B., Peñuelas, J., Shi, X., Stohl, A., Yao, Y., Zhu, Z.
917 and Tans, P. P.: Weakening temperature control on the interannual variations of
918 spring carbon uptake across northern lands, Nature Climate Change, 7(5), 359–
919 363, doi:10.1038/nclimate3277, 2017.
920 Raz-Yaseef, N., Torn, M. S., Wu, Y., Billesbach, D. P., Liljedahl, A. K., Kneafsey, T. J.,
921 Romanovsky, V. E., Cook, D. R. and Wullschleger, S. D.: Large CO2 and CH4
922 emissions from polygonal tundra during spring thaw in northern Alaska,
923 Geophysical Research Letters, 44(1), 504–513, doi:10.1002/2016GL071220,
924 2017.
925 Rydén, B. E., Fors, L. and Kostov, L.: Physical Properties of the Tundra Soil-Water
926 System at Stordalen, Abisko, Ecological Bulletins, (30), 27–54, 1980.
927 Rydén B. E. and Kostov, L.: Thawing and freezing in tundra soil, Ecological Bulletins,
928 (30), 27–54, 1980.
929 Schuur, E. a. G., McGuire, A. D., Schädel, C., Grosse, G., Harden, J. W., Hayes, D. J.,
930 Hugelius, G., Koven, C. D., Kuhry, P., Lawrence, D. M., Natali, S. M., Olefeldt,
931 D., Romanovsky, V. E., Schaefer, K., Turetsky, M. R., Treat, C. C. and Vonk, J.
932 E.: Climate change and the permafrost carbon feedback, Nature, 520(7546), 171–
933 179, doi:10.1038/nature14338, 2015.

Sonesson, M. (1972) Cryptogams. In: International biological programme—Swedish tundra biome project. Technical report No. 9, April 1972. Swedish Natural Science Research Council Ecological Research Committee.

Tokida, T., Miyazaki, T., Mizoguchi, M., Nagata, O., Takakai, F., Kagemoto, A. and Hatano, R.: Falling atmospheric pressure as a trigger for methane ebullition from peatland, Global Biogeochemical Cycles, 21(2), doi:10.1029/2006GB002790, 2007.

Viovy, N.: CRUNCEP Version 7 - Atmospheric Forcing Data for the Community Land Model, Research Data Archive at the National Center for Atmospheric Research, Computational and Information Systems Laboratory, Boulder CO.

Wickland, K. P., Striegl, R. G., Neff, J. C. and Sachs, T.: Effects of permafrost melting on CO2 and CH4 exchange of a poorly drained black spruce lowland, Journal of Geophysical Research: Biogeosciences, 111(G2), doi:10.1029/2005JG000099, 2006.

Woodcroft, B. J., Singleton, C. M., Boyd, J. A., Evans, P. N., Emerson, J. B., Zayed, A. A. F., Hoelzle, R. D., Lamberton, T. O., McCalley, C. K., Hodgkins, S. B., Wilson, R. M., Purvine, S. O., Nicora, C. D., Li, C., Frolking, S., Chanton, J. P., Crill, P. M., Saleska, S. R., Rich, V. I. and Tyson, G. W.: Genome-centric view of carbon processing in thawing permafrost, Nature, doi:10.1038/s41586-018-0338-1, 2018.

Wu, Z., Ahlström, A., Smith, B., Ardö, J., Eklundh, L., Fensholt, R. and Lehsten, V.: Climate data induced uncertainty in model-based estimations of terrestrial

primary productivity, Environmental Research Letters, 12(6), 064013, doi:10.1088/1748-9326/aa6fd8, 2017.

Yoshimura, K. and Kanamitsu, M.: Dynamical Global Downscaling of Global Reanalysis, Monthly Weather Review, 136(8), 2983–2998, doi:10.1175/2008MWR2281.1, 2008.

Zaehle, S., Friend, A. D., Friedlingstein, P., Dentener, F., Peylin, P. and Schulz, M.: Carbon and nitrogen cycle dynamics in the O-CN land surface model: 2. Role of the nitrogen cycle in the historical terrestrial carbon balance, Global Biogeochemical Cycles, 24(1), doi:10.1029/2009GB003522, 2010.

Zimov, S. A., Davydov, S. P., Zimova, G. M., Davydova, A. I., Schuur, E. a. G., Dutta, K. and Chapin, F. S.: Permafrost carbon: Stock and decomposability of a globally significant carbon pool, Geophysical Research Letters, 33(20), doi:10.1029/2006GL027484, 2006.

Table 1. Temporal coverage of quality-controlled $CO_2$ and $CH_4$ exchanges measured by automated chambers at the three peatland types in the Stordalen Mire during the years 2002 to 2007.

| | $CO_2$ | | | $CH_4$ | | |
|---|---|---|---|---|---|---|
| Sites | Number of data points | 3 Hourly coverage (%) | Daily coverage (%) | Number of data points | 3 Hourly coverage (%) | Daily coverage (%) |
| Palsa | 12752 | 65.8 | 12.4 | N/A | N/A | N/A |
| Bog | 12821 | 68.5 | 12.7 | 6660 | 96.2 | 25.0 |
| Fen | 8989 | 63.8 | 13.7 | 4923 | 90.5 | 33.7 |

Note: The temporal coverage represents the percentage of data points that passed our quality-controlled threshold at the corresponding time steps. See main text for threshold details.

Table 2. Evaluation of the 3 hourly and daily $CO_2$ and $CH_4$ exchanges simulated at the palsa, bog, and fen sites.

| | | 3-Hourly | | Daily | |
|---|---|---|---|---|---|
| | | $R^2$ | RRMSE (%) | $R^2$ | RRMSE (%) |
| Sites | C component | | | | |
| Palsa | $CO_2$ | 0.48 | 13.4 | 0.36 | 18.3 |
| Bog | $CO_2$ | 0.63 | 19.1 | 0.44 | 35.8 |
| | $CH_4$ | 0.31 | 16.3 | 0.47 | 22.3 |
| Fen | $CO_2$ | 0.64 | 8.4 | 0.43 | 25.5 |
| | $CH_4$ | 0.44 | 11.1 | 0.54 | 16.9 |

Note: RRMSE is relative root mean squared error.

980 Table 3. Means and standard deviations of cumulative $CO_2$ and $CH_4$ exchanges simulated

981 in the palsa, bog, and fen during the period 2003 to 2007.

| | | Growing season; Days 119–288 | | Non-growing season; Days 1–118 and 289–365 | |
|---|---|---|---|---|---|
| | | Mean | Standard deviation | Mean | Standard deviation |
| Sites | C flux component | | | | |
| Palsa | | | | | |
| | $CO_2$ | -72.70 | 19.10 | 38.89 | 4.09 |
| | $CH_4$ | 0.04 | 0.02 | 0.01 | 0.002 |
| Bog | | | | | |
| | $CO_2$ | -79.59 | 21.46 | 42.89 | 2.16 |
| | $CH_4$ | 3.52 | 0.45 | 0.42 | 0.11 |
| Fen | | | | | |
| | $CO_2$ | -88.65 | 7.26 | 44.41 | 6.13 |
| | $CH_4$ | 10.86 | 3.95 | 0.78 | 0.18 |

982 Note: All gas exchanges are in units of g C $m^{-2}$.

983

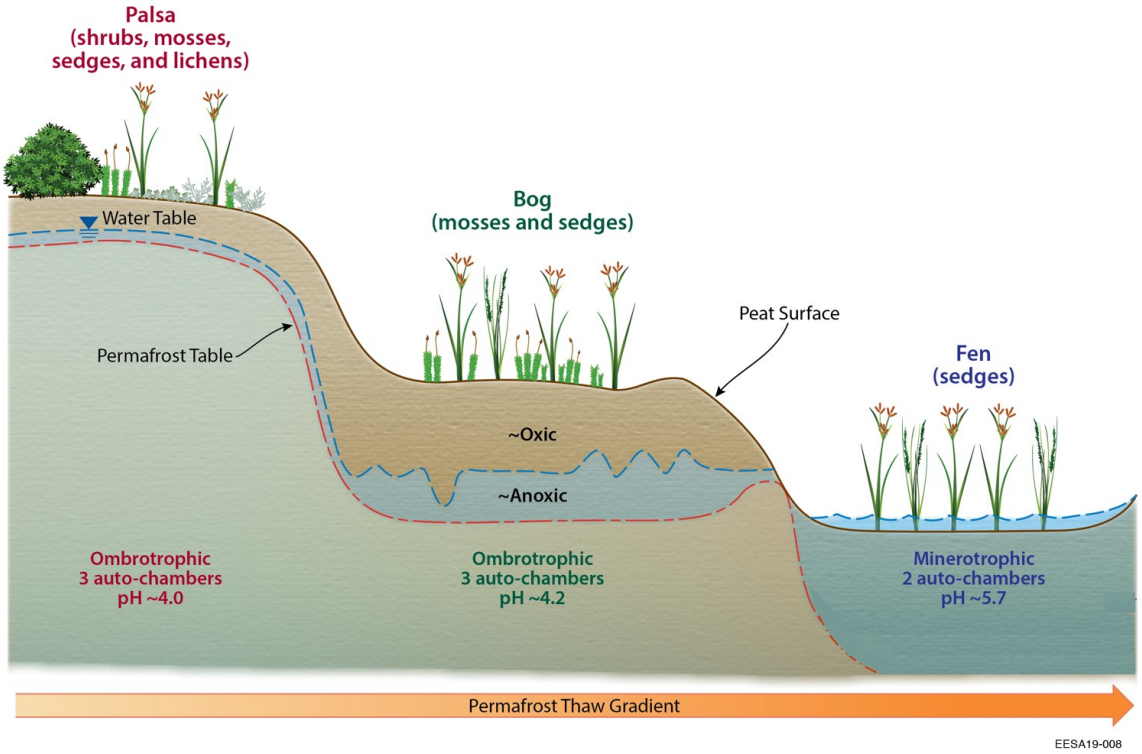


984

985 Figure 1. Schematic diagram of the sampling sites at Stordalen Mire, adapted from

986 Johansson et al. (2006).

987

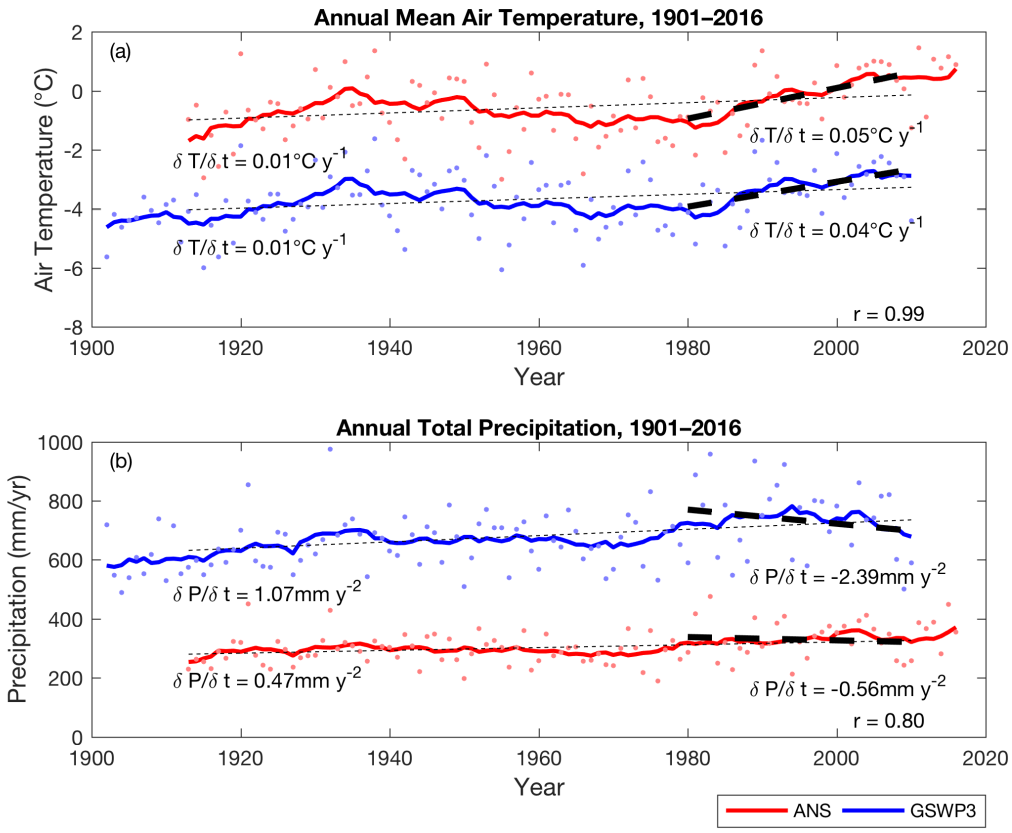


988

989 Figure 2. Time series of air temperature (a) and precipitation (b) measured at ANS (red;
990 years 1913–2016) and extracted from GSWP3 (blue; years 1901–2010). Dots are the
991 annual means and solid lines are the decadal moving averages of the corresponding
992 annual means. Thin and thick dashed lines are the trends for years 1913–2010, and years
993 1980–2010, respectively. The inset r values are the correlation coefficients calculated
994 between the two time series.

995

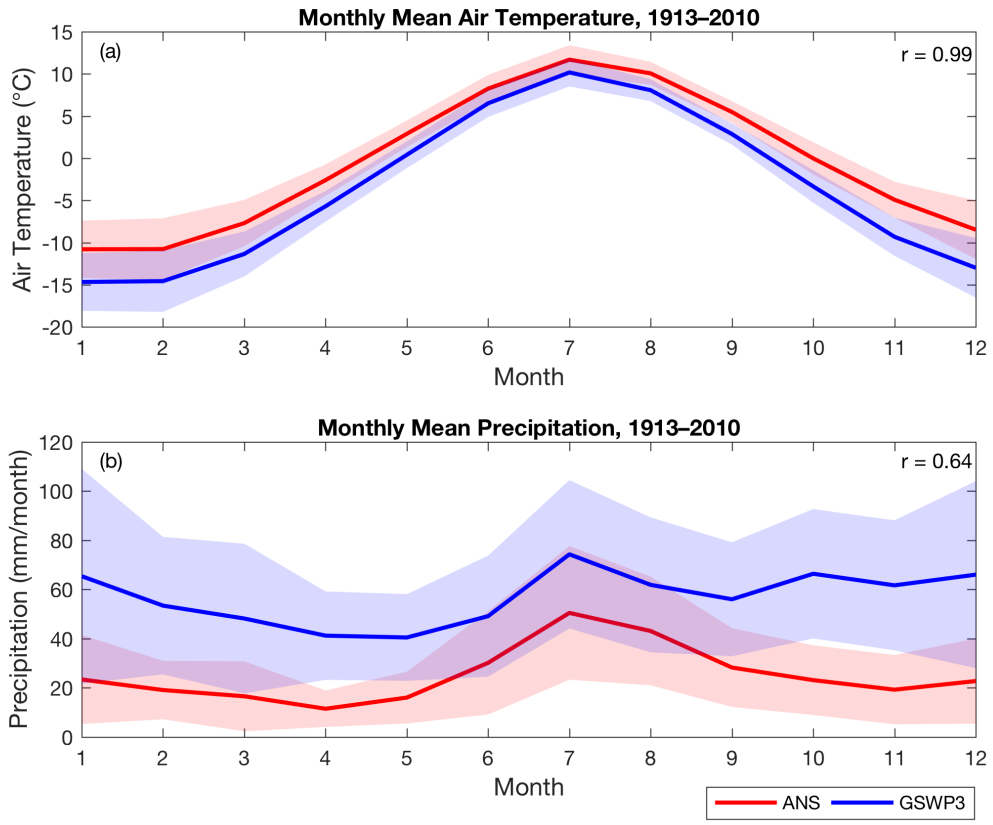


996

997 Figure 3. Monthly mean air temperature (a) and precipitation (b) measured at ANS (red)
998 and extracted from GSWP3 (blue). The shaded area is the inter-annual variability for the
999 corresponding dataset, represented by the standard deviations calculated at each month.
1000 The inset r values are the correlation coefficients calculated between the two time series.

1001

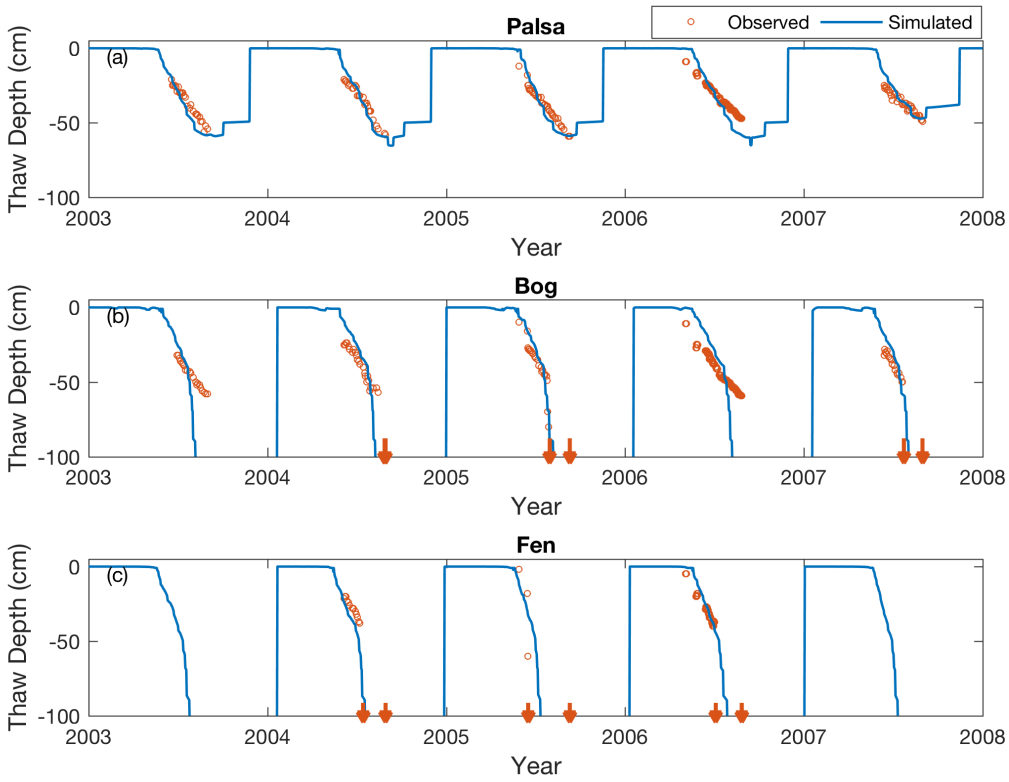


1002

1003 Figure 4. Simulated (solid lines) and measured (open circles) seasonal dynamics of thaw

1004 depth at the palsa (a), bog (b), and fen (c) sites from 2003 to 2007. Downward arrows

1005 indicate the time when measured thaw depth exceeds 90 cm for a measurement year.

1006

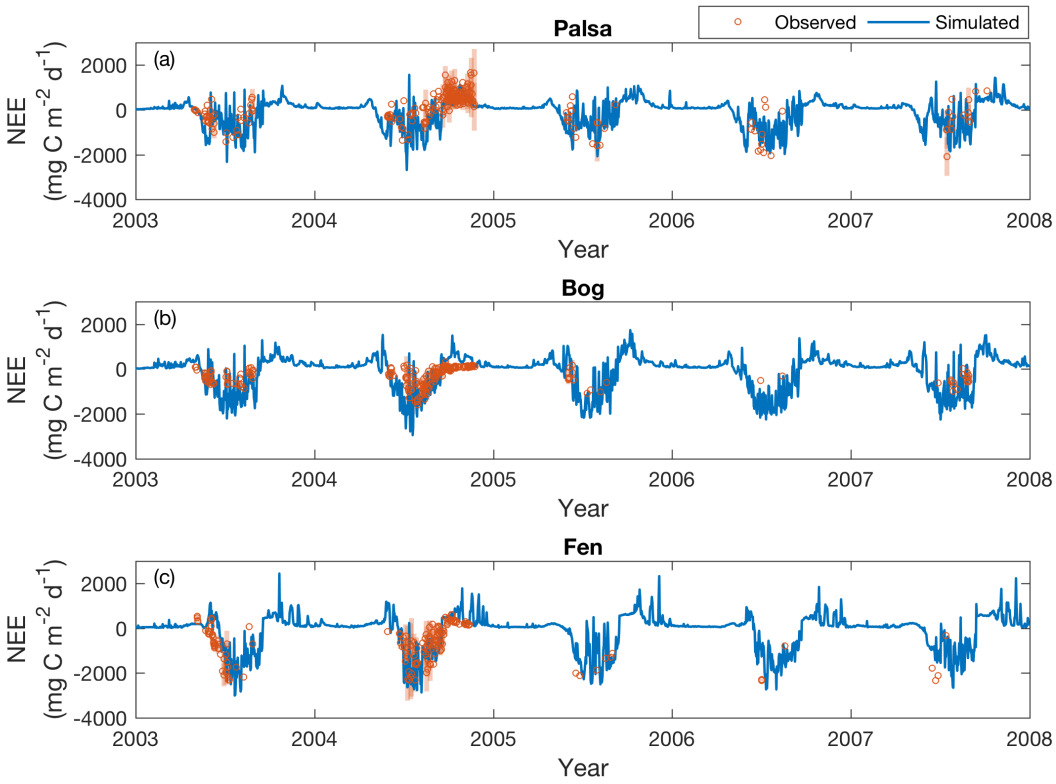


1007

1008 Figure 5. Simulated (solid lines) and measured (open circles) daily $CO_2$ exchanges (NEE)

1009 at the palsa (a), bog (b), and fen (c) sites, from 2003 to 2007. Shaded bars are the

1010 standard deviations of daily NEE measured across subsites under each peatland type.

1011 Positive and negative values indicate effluxes from and influxes to the site, respectively.

1012

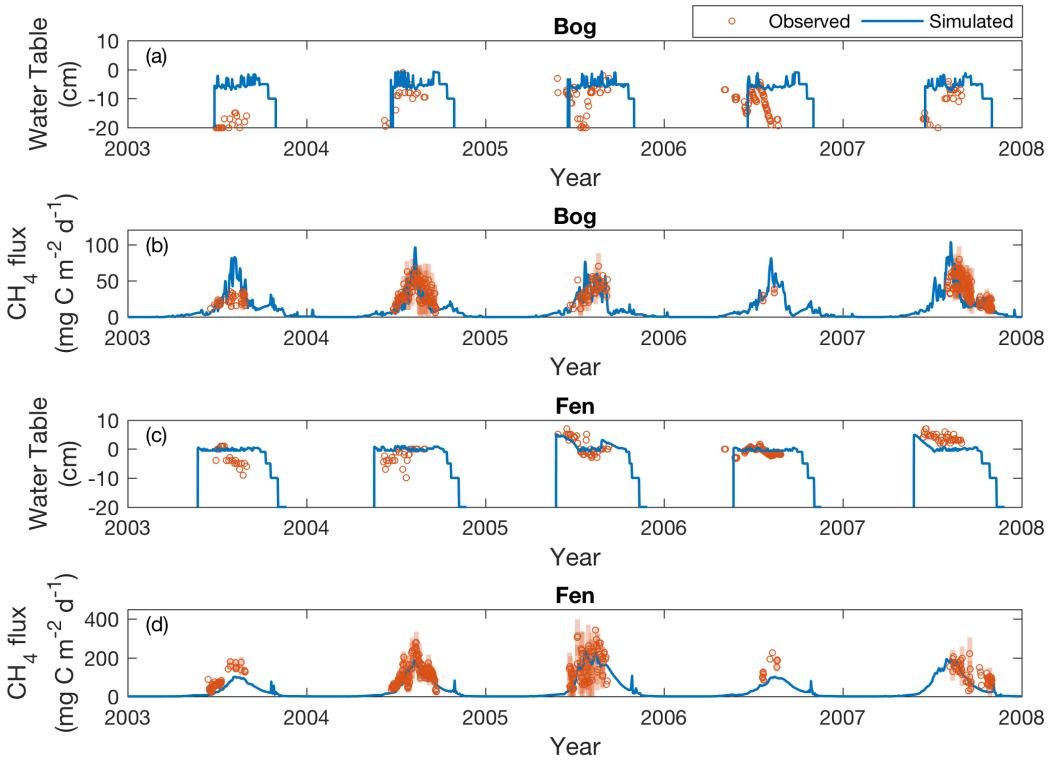


1013

1014 Figure 6. Simulated (solid lines) and measured (open circles) water table depths and daily

1015 $CH_4$ emissions at the bog and fen from 2003 to 2007. Shaded bars are the standard

1016 deviations of the daily $CH_4$ emissions measured across the subsites under each peatland

1017 type.

1018

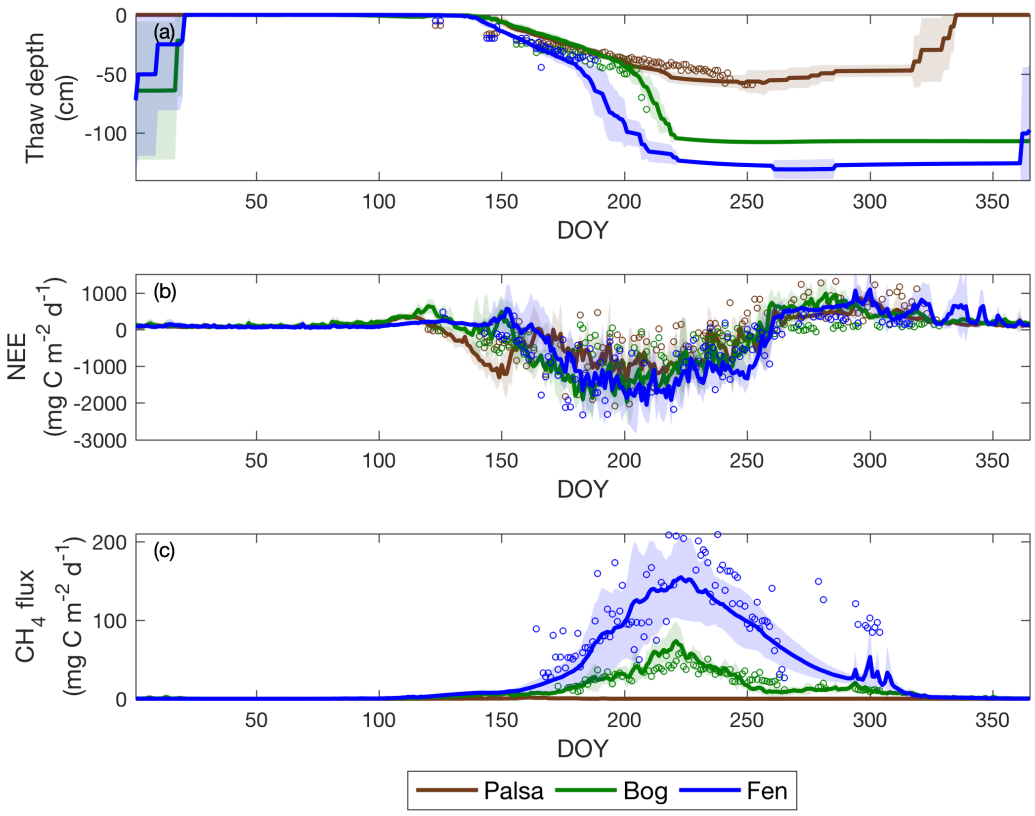


1019

1020 Figure 7. Daily thaw depth (a), daily NEE (b), and daily $CH_4$ (c) exchanges for the three

1021 sites from 2003 to 2007. Solid lines and open circles are the simulated and measured

1022 inter-annual means for each day of year, respectively. The shaded area is the simulated

1023 inter-annual variability for the corresponding dataset, represented by the standard

1024 deviations calculated at each day of year. Positive and negative carbon flux values

1025 indicate effluxes from and influxes to the site, respectively.

1026

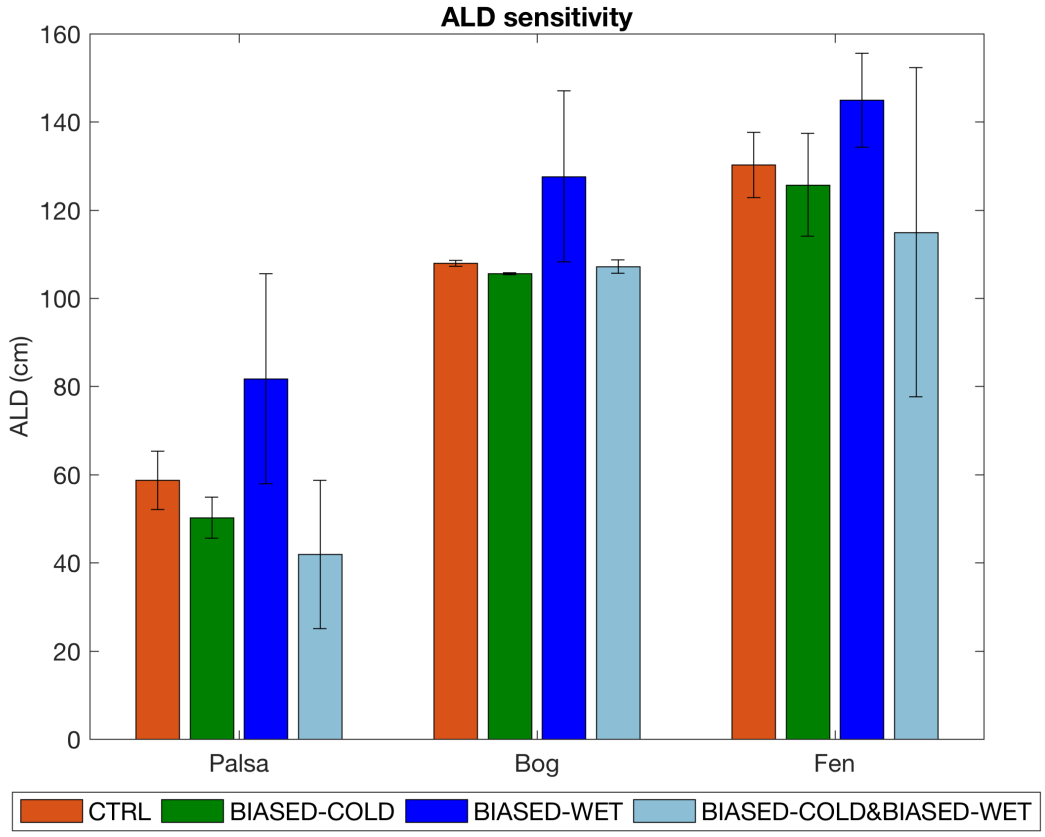


Figure 8. Simulated ALD at the palsa, bog, and fen for four sets of climate forcing (Section 2.5). Bars and error bars are means and standard deviations calculated from 2003 to 2007, respectively.

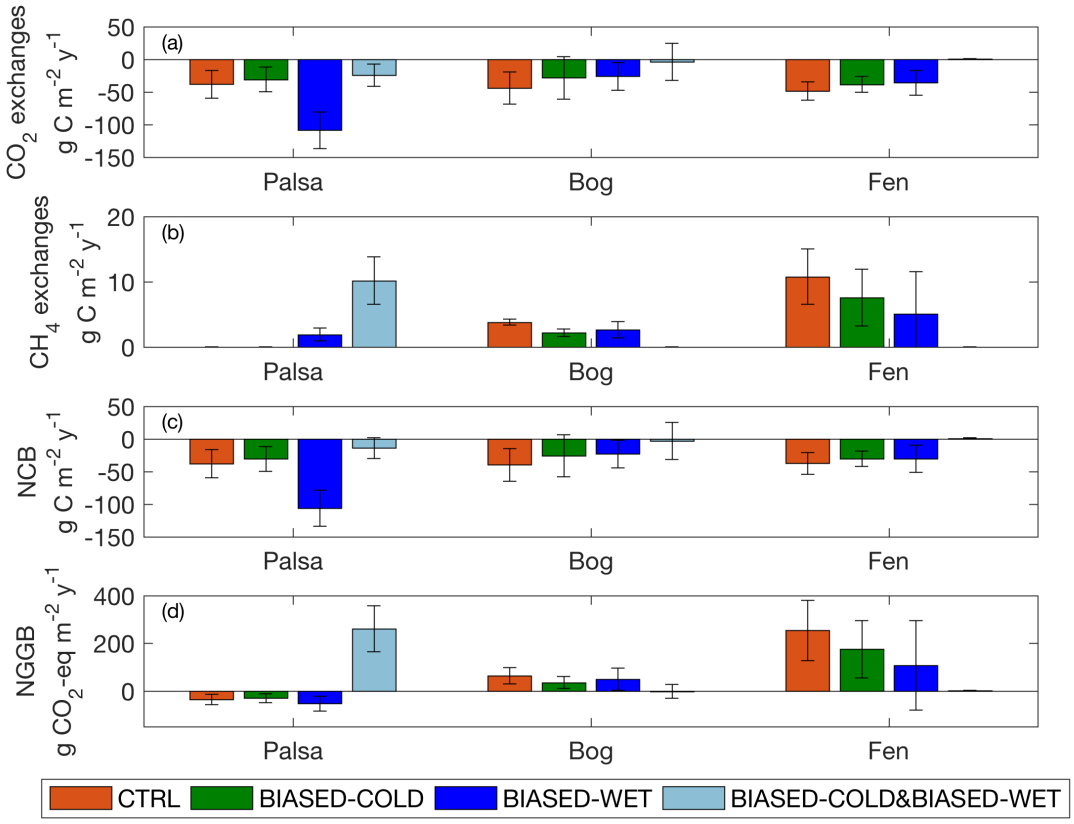


1033

1034 Figure 9. Annual $CO_2$ exchanges (a), $CH_4$ exchanges (b), Net Carbon Balance (c), and

1035 Net Greenhouse Gas Balance (d) simulated at the palsa, bog, and fen, under each set of

1036 simulations. Bars and error bars are the means and standard deviations calculated from

1037 2003 to 2007, respectively. Positive and negative values indicate effluxes from and

1038 influxes to the site, respectively.

1039

1040